14). This protection is most likely due to reduced lipid uptake by adipose tissue because whole-body lipid uptake is markedly decreased in VLDLR-deficient mice. These results suggest that apoE-VLDLR interaction plays an important role in the development of obesity.

PPARγ is the key transcriptional regulator of adipogenesis and directly activates many genes involved in lipid storage (15–17). PPARγ is highly expressed in WAT and is required for adipocyte differentiation (18, 19). PPARγ forms a heterodimer with retinoid X receptor α, and PPARγ/retinoid X receptor α heterodimer binds to a PPRE, containing direct repeats of the hexanucleotide sequence AGGTCA separated by one nucleotide (20). This motif, known as a direct repeat 1 (DR-1) element, is found in the promoter regions of many genes involved in lipid storage, such as the fatty acid-binding protein aP2 and the cholesterol and fatty acid transporter FATP/CD36 (21). Thiazolidinediones (TZDs) are insulin-sensitizing antidiabetic drugs that activate the PPARγ (22). TZDs have also been reported to stimulate adipogenesis by up-regulating many of the PPARγ target genes involved in fatty acid metabolism and storage (23). In fact, numerous studies in rodent models and in humans have shown that treatment with TZDs causes weight gain (24, 25). Although it has been reported that VLDL increases PPARγ expression in cultured adipocytes (1), the possible role of PPARγ in regulation of VLDLR expression and VLDLR-mediated lipid accumulation in adipocytes remains unclear.

In this study, we investigated the effect of rosiglitazone, a PPARγ agonist, on regulation of VLDLR expression both in WAT of obese mice and in cultured adipocytes. Furthermore, to determine whether rosiglitazone directly regulates transcription of the VLDLR gene, we carried out luciferase assay with a reporter gene containing mouse VLDLR promoter region. Our results showed that rosiglitazone increased the expression of VLDLR both in WAT of obese mice and in cultured adipocytes, that functional PPRE existed in the VLDLR promoter region, and that VLDLR was a direct PPARγ target gene. Further *in vivo* experiments showed that rosiglitazone did not increase body weight and WAT weight in apoE-deficient ob/ob mice, but it significantly increased these two parameters in ob/ob mice. In addition, rosiglitazone did not increase body weight and WAT weight in VLDLR-deficient mice. These findings indicate that VLDLR-mediated apoE-containing VLDL uptake plays an important role in rosiglitazone-induced lipid accumulation in adipocytes.

EXPERIMENTAL PROCEDURES

Chemicals—Rosiglitazone was synthesized as described elsewhere (22). All other materials were obtained from sources as described previously (26, 27).

Experimental Animals—The male ob/ob mice were purchased from Charles River Japan (Yokohama, Japan). The male wild-type mice, apoE-deficient mice, ob/ob mice, and apoE-deficient ob/ob mice used in this study, which were prepared by intercross of *apoE*$^{+/-}$ob/+ mice, were all of a C57B6/j background. The male nontransgenic wild-type mice and VLDLR-deficient mice, which were B6;129 background, were obtained from The Jackson Laboratory (Bar Harbor, ME). Mice were housed under a 12-h light/dark cycle in an animal room maintained at 25 °C. Mice were fed a normal chow diet until 6–8 weeks of age, and they were given a high fat diet (32% safflower oil, 33.1% casein, 17.6% sucrose, and 5.6% cellulose (28)) starting 1 week before rosiglitazone administration.

Drug Administration—Rosiglitazone was given as a 0.01% food admixture. The mean dose of rosiglitazone was estimated to be 10 mg/kg/day. This dose was chosen because it has been shown to be the effective therapeutic dose in diabetic mice (24, 29). The ob/ob mice were fed either a high fat diet or a high fat diet with 0.01% rosiglitazone for 4 days. The wild-type mice, apoE-deficient mice, ob/ob mice, and apoE-deficient ob/ob mice were fed either a high fat diet or a high fat diet with 0.01% rosiglitazone for 10 weeks. The wild-type mice and VLDLR-deficient mice were fed either a high fat diet or a high fat diet with 0.01% rosiglitazone for 7 weeks.

Blood Sample Assays and in Vivo Glucose Homeostasis—The oral glucose tolerance test was performed by oral gavages of 0.75 g/kg of body weight glucose after 24 h of fasting followed by blood sampling at 0, 15, 30, 60, and 120 min. An insulin tolerance test was performed by 1.5 units/kg of body weight of intraperitoneal insulin followed by blood sampling at the 0, 30, 60, and 90 min (26). Plasma glucose was determined by a glucose test (Wako Pure Chemical Industries, Osaka, Japan). Plasma insulin was measured by an insulin immunoassay (Shibayagi, Gunma, Japan), and plasma adiponectin concentration was determined by a mouse adiponectin immunoassay kit (Otsuka Pharmaceutical, Tokushima, Japan).

Histological Analysis of Adipose Tissue—Epididymal WAT was removed from each animal, fixed in 10% formaldehyde/phosphate-buffered saline, and maintained at 4 °C until use. Fixed specimens were dehydrated, embedded in tissue-freezing medium (Tissue-Tek OCT compound; Miles, Elkhart, IN), and frozen in dry ice and acetone. WAT was cut into 10-μm sections, and the sections were mounted on silanized slides. The adipose tissue was stained with hematoxylin and eosin (30).

RNA Analysis of Mouse 3T3-L1 Adipocytes and Tissues—Mouse 3T3-L1 cells were grown in Dulbecco's modified Eagle's medium high glucose supplemented with 10% fetal bovine serum. Induction of adipocyte differentiation was carried out according to a method described previously (31). On 7 days after the induction of differentiation, 3T3-L1 adipocytes were incubated at 37 °C with rosiglitazone and pioglitazone in Dulbecco's modified Eagle's medium high glucose supplemented with 10% fetal bovine serum for 24 h. The cells were harvested to isolate total RNA. Total RNA was isolated from cells or tissues with TRIzol (Invitrogen) according to the manufacturer's instructions. For quantification of mRNA, we conducted a real-time PCR using an ABI prism 7900 and sets of primer and probe for each gene (Applied Biosystems, Foster City, CA). The relative amount of each transcript was normalized to the amount of β-actin and 36B4 transcript in the same cDNA (32).

Western Blotting—On 7 days after the induction of differentiation, 3T3-L1 adipocytes were incubated with 1 μM rosiglitazone for 24 h. Total cellular protein (10 μg) from cells was subjected to SDS-PAGE and transferred to polyvinylidene difluoride membranes. Anti-VLDLR antibody (6A6) and horseradish peroxidase-conjugated anti-mouse IgG (Santa Cruz Biotechnology, Santa Cruz, CA) were used to probe for VLDLR

protein. Bands were detected with the ECL Plus Western blotting detection kit (GE Healthcare) according to the manufacturer's instructions.

Luciferase Reporter Assay—To generate luciferase reporter plasmids of mouse VLDLR promoter, PCR fragments (−2590 to −1 bp) from the mouse genomic DNA were inserted into the BglII and NcoI sites of the pGL3 basic luciferase expression vector (Promega, Madison, WI). Point mutation of the pGL3-VLDLR luciferase plasmid was introduced using the GeneTailor system (Invitrogen). On 3 days after the induction of differentiation, 3T3-L1 adipocytes were transfected with luciferase reporter plasmids using Lipofectamine Plus (Invitrogen) according to the instructions provided by the manufacturer. After transfection, the cells were incubated in a medium containing rosiglitazone, pioglitazone, or DMSO. At 16 h after ligand treatment, luciferase reporter assay were performed using the Luciferase Assay System (Promega).

EMSA—The nuclear proteins were extracted from 3T3-L1 adipocytes on 7 days after differentiation using the CelLytic NuCLEAR extraction kit (Sigma) according to the manufacturer's instructions. EMSA was performed using the gel shift assay systems (Promega). The sequences of double-stranded oligonucleotides were as follows (only one strand is shown, and the half-site of the putative PPRE and the mutated PPRE are underlined). Mouse VLDLR PPRE, 5′-TGATTTCAGTTTACAGGTCAGATGGCAGGCACAG-3′; mouse VLDLR mutant PPRE, 5′-TGATTTCGGTTTACATCGTTGATGGCTGGCACAG-3′. Double-stranded oligonucleotides were radioactively end-labeled with [γ-^{33}P]dATP (PerkinElmer Life Sciences) using T4 polynucleotide kinase (Promega) and purified from unincorporated nucleotides by gel filtration through G-25 spin columns (GE Healthcare). All of the EMSA reactions were carried out according to the manufacturer's instructions using 2 μg of nuclear extracts. DNA-protein complexes were resolved by electrophoresis through 6% polyacrylamide gels in 0.5× Tris borate running buffer (Bio-Rad). For the competition assay, a 50-fold amount of unlabeled double-stranded DNAs was added in the binding reaction. For supershift assays, nuclear extracts were preincubated with 2 μg of mouse monoclonal anti-PPARγ antibody (E8) (Santa Cruz Biotechnology) or with 2 μg of mouse control IgG (Santa Cruz Biotechnology) for 10 min before the oligonucleotides were added.

ChIP Assay—On 4 days after the induction of differentiation, 3T3-L1 adipocytes were incubated with 1 μM rosiglitazone for 24 h. The DNA and protein were cross-linked with 1% formaldehyde for 10 min. Soluble chromatin was prepared using the ChIP assay kit (Upstate Biotechnology, Lake Placid, NY). After sonication, lysates were precipitated with rabbit polyclonal anti-PPARγ antibody (H100) and normal rabbit IgG (Santa Cruz Biotechnology) according to the manufacturer's instructions. Primers used for ChIP PCR were as follows: VLDLR-PPRE forward, 5′-TGAGGCCACAGATGATTTTG-3′; VLDLR-PPRE reverse, 5′-GGCTCTACACTCAACCTG-GTG-3′; aP2-PPRE forward, 5′-ATGTCACAGGCATCTTA-TCCACC-3′; aP2-PPRE reverse, 5′-AACCCTGCCAAAGAG-ACAGAGG-3′; negative control primer forward, 5′-CTCCC-CGATCACTGGAATAG-3′; and negative control primer reverse, 5′-ACCCTAGAGACACTGGTGGTG-3′. The negative control primers are located ~2 kbp upstream of the PPRE for VLDLR. PCR was performed for 45 cycles. PCR products were analyzed by 2% agarose gel electrophoresis.

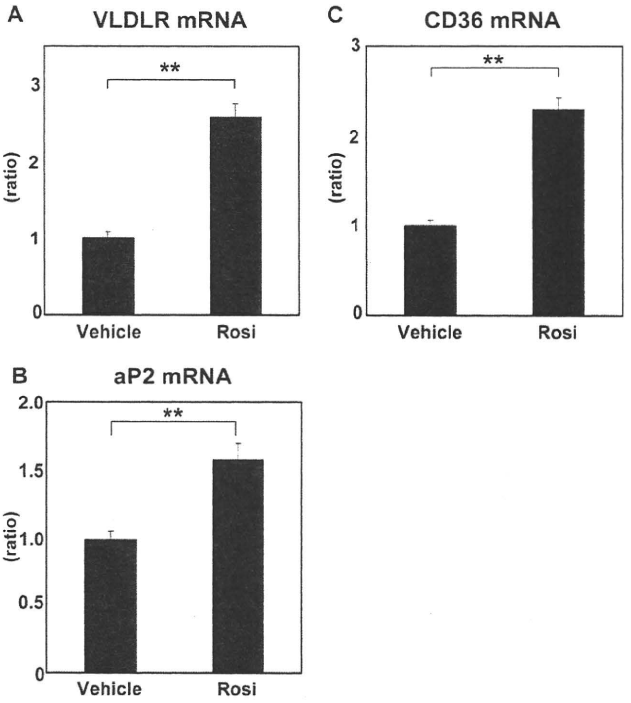

FIGURE 1. **Effects of rosiglitazone treatment for 4 days on gene expression of molecules involved in lipid metabolism in WAT from ob/ob mice.** *A–C*, amounts of the mRNAs of VLDLR (*A*), aP2 (*B*), and CD36 (*C*) in epididymal WAT of ob/ob mice treated with vehicle or 0.01% rosiglitazone (*Rosi*) as food admixture for 4 days while on the high fat diet. The mRNA levels of molecules indicated above were quantified by a real-time PCR method as described under "Experimental Procedures." The relative amount of each transcript was normalized to the amount of 36B4 transcript in the same cDNA. The results are expressed as the ratio of the value of ob/ob mice. Each bar represents the means ± S.E. (*error bars*; $n = 5$). **, $p < 0.01$.

RESULTS

Rosiglitazone Increases the Expression of VLDLR in Adipose Tissue of ob/ob Mice—Previous studies have shown that rosiglitazone enhances lipid accumulation in adipose tissue by up-regulating many of the PPARγ target genes involved in fatty acid metabolism and storage (24, 25). In addition, it has been reported that VLDLR is one of the key molecules for the development of obesity (13, 14). To investigate the effect of rosiglitazone on the expression of VLDLR, we treated ob/ob mice, while on the high fat diet, with rosiglitazone (0.01% food admixture) for 4 days and examined VLDLR gene expression in WAT using quantitative PCR analysis. We also examined the effect of rosiglitazone on the expression of aP2 and CD36, which are target genes of PPARγ, in WAT of ob/ob mice. Rosiglitazone significantly increased the expression of VLDLR in WAT of ob/ob mice by 2.6-fold as compared with the vehicle (Fig. 1*A*). In addition, treatment with rosiglitazone significantly increased the expression of aP2 and CD36 in WAT of

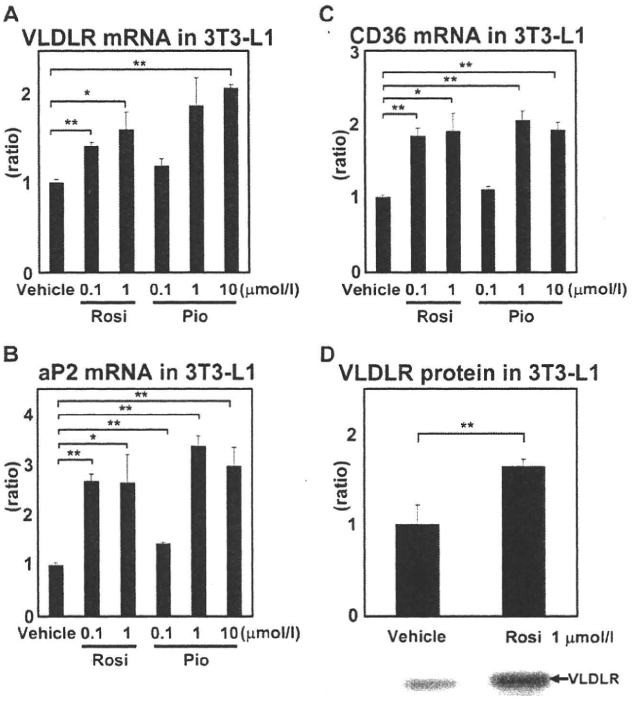

FIGURE 2. **Effects of rosiglitazone on expression of VLDLR in cultured cells.** *A–D*, amounts of mRNAs of VLDLR (*A*), aP2 (*B*), and CD36 (*C*) from 3T3-L1 adipocytes incubated with vehicle, rosiglitazone (*Rosi*), or pioglitazone (*Pio*) for 24 h and amounts of VLDLR protein (*D*) from 3T3-L1 adipocytes incubated with vehicle or 1 μM rosiglitazone for 24 h. The mRNA levels of molecules indicated above were quantified by a real-time PCR method as described under "Experimental Procedures." The relative amount of each transcript was normalized to the amount of 36B4 transcript in the same cDNA. Immunoblot analysis was performed using anti-VLDLR antibody. The results are expressed as the ratio of the value of vehicle. Each bar represents the means ± S.E. (*error bars*, $n = 3$). *, $p < 0.05$, **, $p < 0.01$.

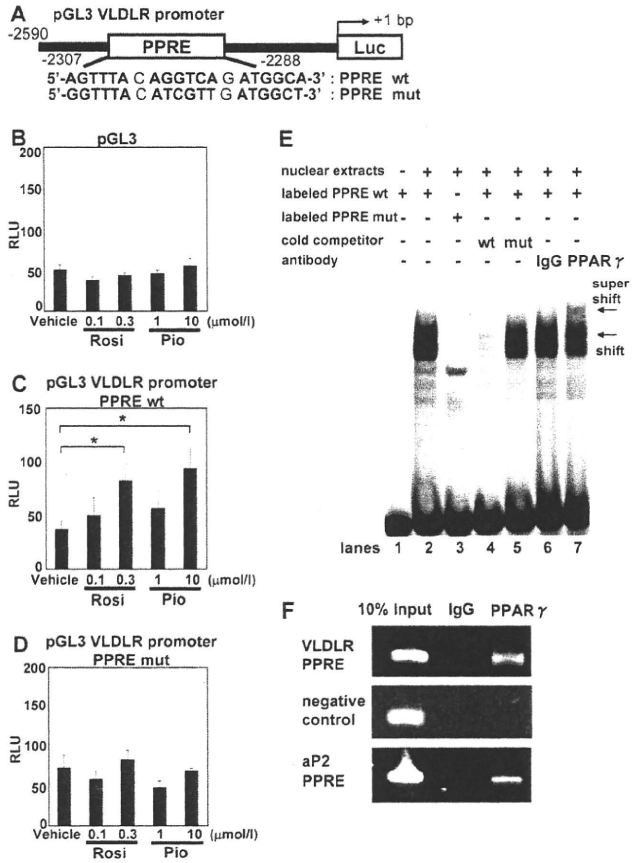

FIGURE 3. **Identification of functional PPRE in mouse VLDL promoter region.** *A*, the luciferase (*Luc*) reporter plasmid was generated by inserting mouse VLDLR promoter region (−2590 to −1 bp: the transcription start site is +1) into the pGL3 basic luciferase expression vector. PPRE sequence at position −2307 to −2288 is indicated. Some mutations (*mut*) were introduced in the PPRE. *B–D*, on 3 days after the induction of differentiation, 3T3-L1 adipocytes were transfected with luciferase reporter plasmids. after transfection, the cells were incubated with a medium containing rosiglitazone (*Rosi*), pioglitazone (*Pio*), or DMSO. At 16 h after ligand treatment, a luciferase reporter assay was performed. Transcriptional activity was compared among pGL3, pGL3 VLDLR promoter PPRE wild type, and pGL3 VLDLR promoter PPRE mutant. Each bar represents the means ± S.E. (*error bars*, $n = 3–5$). *, $p < 0.05$. *E*, EMSA was performed on double-stranded oligonucleotides corresponding to the mouse VLDLR PPRE and mutant PPRE. *Lane 1*, radiolabeled VLDLR-PPRE oligonucleotides alone; *lane 2*, radiolabeled VLDLR-PPRE oligonucleotides with nuclear extract; *lane 3*, radiolabeled VLDLR-PPRE mutant oligonucleotides with nuclear extract. Unlabeled oligonucleotides of VLDLR-PPRE (*lane 4*) and VLDLR-PPRE mutant (*lane 5*) were added as competitor to the condition of the *lane 2*. IgG (*lane 6*) or anti-PPARγ antibody (*lane 7*) was also added as competitor to the condition of the *lane 2*. *F*, ChIP analysis of PPARγ association with VLDLR gene was conducted. The negative control primers are located ~2 kbp upstream of the PPRE in the VLDLR promoter region.

ob/ob mice by 1.6- and 2.3-fold, respectively, as compared with the vehicle (Fig. 1, *B* and *C*).

Rosiglitazone Regulates VLDLR Expression in 3T3-L1 Adipocytes—To confirm that the VLDLR gene is a target of PPARγ, we examined the effect of rosiglitazone on the expression of VLDLR in cultured 3T3-L1 adipocytes. Rosiglitazone increased the expression of VLDLR in a dose-dependent manner (Fig. 2*A*). The expression of aP2 and CD36, which have functional PPREs in their promoter regions, was also increased by treatment with rosiglitazone (Fig. 2, *B* and *C*). Furthermore, rosiglitazone significantly increased VLDLR protein levels as well as mRNA levels (Fig. 2*D*). These findings indicate that rosiglitazone directly increases VLDLR expression in 3T3-L1 adipocytes. We also examined the effect of another TZD, pioglitazone, on the expression of VLDLR in 3T3-L1 adipocytes. Pioglitazone also increased the expression of VLDLR in 3T3-L1 adipocytes (Fig. 2*A*), and its effect was comparable with that of rosiglitazone.

Rosiglitazone Directly Enhances Transcription of the VLDLR Gene—To determine whether rosiglitazone directly regulates transcription of the VLDLR gene via a PPRE in its promoter region, we carried out a luciferase assay with a reporter gene including mouse VLDLR promoter region (Fig. 3*A*). A luciferase reporter construct containing the VLDLR promoter region was transfected into 3T3-L1 adipocytes 3 days after induction of differentiation. Incubation with rosiglitazone, as well as with pioglitazone, for 16 h significantly enhanced VLDLR promoter transcriptional activity by 2.3-fold as compared with incubation with the vehicle (Fig. 3, *B* and *C*). This result indicates that the element responsible for rosiglitazone- or pioglitazone-induced transcriptional activity is included in the VLDLR promoter region. Inspection of this region revealed a putative PPRE of the DR1 type at −2307 to −2288 bp (Fig. 3*A*). To determine whether this putative PPRE is involved in the rosiglitazone-mediated regulation of VLDLR gene expression, luciferase reporter constructs containing wild-type or PPRE-mutated

mouse VLDLR promoter were transfected into 3T3-L1 adipocytes (Fig. 3, *B–D*). Transfection of the PPRE-mutated reporter construct resulted in a remarkable suppression of rosiglitazone-induced increase in luciferase activity (Fig. 3*D*). This result suggests that the PPRE motif in VLDLR promoter plays a significant role in transcriptional activation of the VLDLR gene in adipocytes.

Endogenous PPARγ Directly Binds to the PPRE Motif in VLDLR Promoter Region—To determine whether PPARγ directly binds to the PPRE motif in the VLDLR promoter region in adipocytes, we carried out EMSA. Incubation of nuclear extract from differentiated 3T3-L1 adipocytes with a radiolabeled double-stranded oligonucleotide containing the putative PPRE motif in the VLDLR promoter region resulted in a shifted complex that was effectively competed by wild-type but not mutant PPRE (Fig. 3*E*, *lanes 1*, *2*, *4*, and *5*). In addition, incubation of the 3T3-L1 nuclear extracts with monoclonal antibody against PPARγ supershifted the complex to the higher molecular weight position (Fig. 3*E*, *lanes 6* and *7*). On the other hand, a radiolabeled double-stranded oligonucleotide containing the mutant PPRE in the VLDLR promoter region did not form a complex with nuclear extracts (Fig. 3*E*, *lane 3*). These results indicate that the shifted complex contains the endogenous PPARγ at least in part. We next used the ChIP assay to study the transcriptional regulation of the endogenous VLDLR gene in 3T3-L1 adipocytes. Primer sets were designed to span the PPRE motif. ChIP analysis demonstrated that PPARγ bound in the region of the PPRE in VLDLR promoter, whereas a region ~2 kbp upstream of the PPRE showed no binding of PPARγ (Fig. 3*F*). As expected, the aP2 promoter region containing its PPRE was also bound by PPARγ (Fig. 3*F*). Thus, these results suggest that PPARγ directly binds in the region of functional PPRE in VLDLR promoter.

Rosiglitazone Does Not Increase Body Weight and WAT Weight in ApoE-deficient ob/ob Mice—It has previously been reported that VLDLR recognizes apoE-containing lipoprotein and mediates lipid uptake in adipose tissue (10, 11). To clarify whether the regulation of VLDLR-mediated apoE-containing VLDL uptake into adipocytes is responsible for rosiglitazone-induced weight gain, we next examined the effect of rosiglitazone on body weight and WAT weight in apoE-deficient ob/ob mice, in which VLDLR cannot recognize apoE-deficient VLDL particles. In our experiment, ob/ob mice and apoE-deficient ob/ob mice, while on the high fat diet, were treated with rosiglitazone (0.01% food admixture) for 10 weeks. Rosiglitazone significantly increased both body weight and WAT weight in ob/ob mice (Fig. 4, *A–C*). In contrast, no significant difference in body weight and WAT weight was observed between rosiglitazone-treated apoE-deficient ob/ob mice and the vehicle-treated apoE-deficient ob/ob mice (Fig. 4, *A–C*). These results indicate that apoE-dependent lipid uptake into adipocytes, at least in part, contributes to WAT weight gain by rosiglitazone.

Rosiglitazone Ameliorates Insulin Resistance in ApoE-deficient ob/ob Mice—We also examined the antidiabetic effect of rosiglitazone in apoE-deficient ob/ob mice. As shown in Fig. 5, *A–C*, both blood glucose and plasma insulin concentrations, measured in a glucose tolerance test, in rosiglitazone-treated apoE-deficient ob/ob mice were lower than those in the vehicle-treated apoE-deficient ob/ob mice. In addition, insulin resistance index in rosiglitazone-treated apoE-deficient ob/ob mice decreased by 42% as compared with that in the vehicle-treated apoE-deficient ob/ob mice. Furthermore, blood glucose concentration, measured in the insulin tolerance test, in rosiglitazone-treated apoE-deficient ob/ob mice was significantly lower than that in the vehicle-treated apoE-deficient ob/ob mice. The extent of improvement in blood glucose and plasma insulin concentrations caused by rosiglitazone in apoE-deficient ob/ob mice was comparable with that in ob/ob mice (Fig. 5, *D* and *E*). These results indicate that treatment with rosiglitazone ameliorates glucose intolerance and insulin resistance in apoE-deficient ob/ob mice and that these effects of rosiglitazone may not depend on the apoE-VLDLR pathway.

We have previously shown that PPARγ activation by a TZD prevents adipocyte hypertrophy (33) and increases plasma adiponectin concentration, which results in amelioration of insulin resistance (30, 34). Accordingly, we examined in this study the effect of rosiglitazone on adipocyte size in apoE-deficient ob/ob mice. Although treatment with rosiglitazone increased the number of small adipocytes in WAT of ob/ob mice, there was no significant difference in adipocyte size in WAT of apoE-deficient ob/ob mice between treatment with the vehicle and that with rosiglitazone (Fig. 6, *A* and *C*). On the other hand, plasma adiponectin concentration in both ob/ob mice and

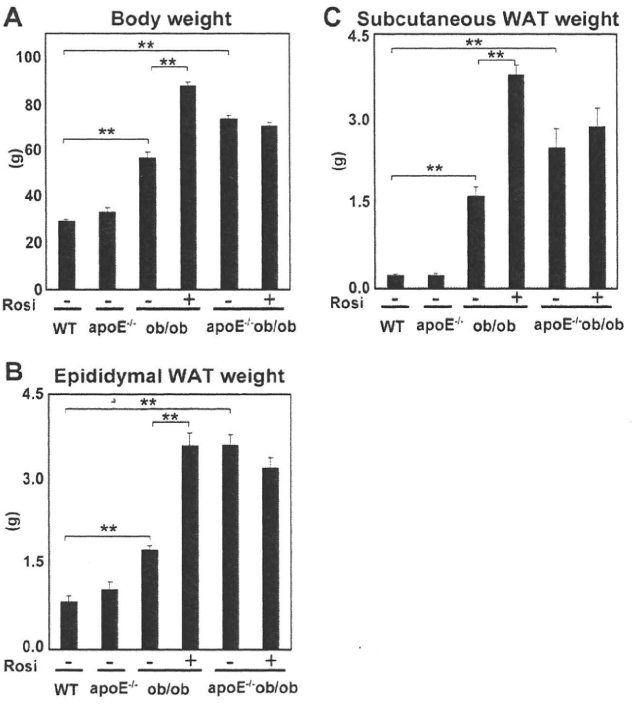

FIGURE 4. **Effects of rosiglitazone treatment for 10 weeks on body weight and WAT weight in ob/ob mice and apoE-deficient ob/ob mice.** *A–C*, body weight (*A*), epididymal WAT weight (*B*), and subcutaneous WAT weight (*C*). Wild-type mice (WT), apoE-deficient mice ($apoE^{-/-}$), ob/ob mice, and apoE-deficient ob/ob mice ($apoE^{-/-}$ ob/ob) were fed with the high fat diet for 10 weeks, and ob/ob mice and $apoE^{-/-}$ ob/ob mice were treated with 0.01% rosiglitazone (*Rosi*) as food admixture for 10 weeks while on the high fat diet. Each bar represents the means ± S.E. (*error bars*, $n = 5$, WT mice and $apoE^{-/-}$ mice, $n = 4$: ob/ob mice, ob/ob mice treated with rosiglitazone and $apoE^{-/-}$ ob/ob mice, $n = 3$: $apoE^{-/-}$ ob/ob mice treated with rosiglitazone). *, $p < 0.05$, **, $p < 0.01$.

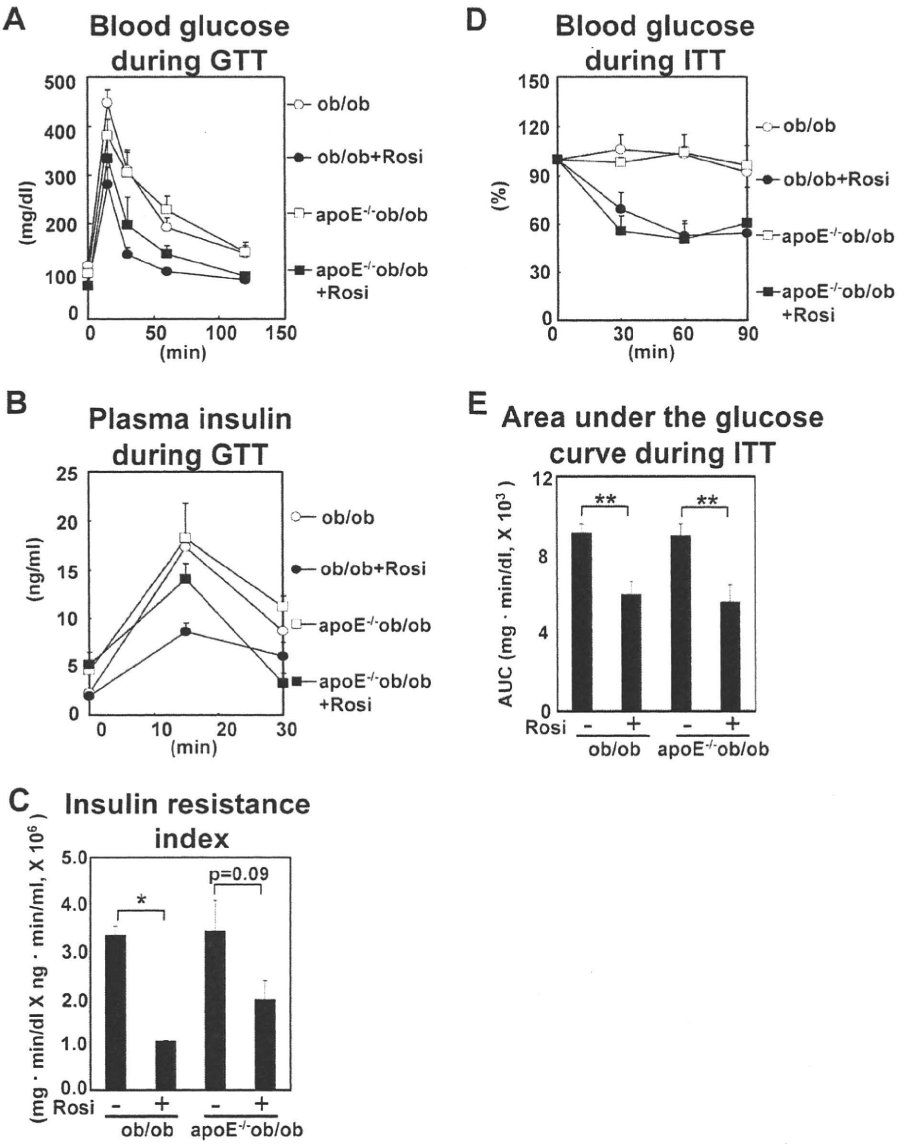

FIGURE 5. **Effects of rosiglitazone treatment for 10 weeks on glucose tolerance and insulin sensitivity in ob/ob mice and apoE-deficient ob/ob mice.** *A–C*, blood glucose concentration and plasma insulin concentration (*A* and *B*) and insulin resistance index (area under the curve (*AUC*) of blood glucose × AUC of blood insulin) (*C*) during an oral glucose tolerance test (*GTT*) of ob/ob mice and apoE-deficient ob/ob mice (*apoE*$^{-/-}$ ob/ob) treated with vehicle or 0.01% rosiglitazone (*Rosi*) as food admixture for 10 weeks while on the high fat diet. *D* and *E*, blood glucose concentration during an insulin tolerance test (*ITT*) of ob/ob mice and *apoE*$^{-/-}$ ob/ob mice treated with vehicle or 0.01% rosiglitazone as food admixture for 10 weeks while on the high fat diet. An oral glucose tolerance test was performed by oral gavages of 0.75 g/kg of body weight glucose after 24 h of fasting followed by blood sampling at the indicated time. An insulin tolerance test was performed by 1.5 units/kg of body weight of intraperitoneal insulin followed by blood sampling at the indicated time. Each bar represents the means ± S.E. (*error bars*) ($n = 4$, ob/ob mice (*closed circles*) and *apoE*$^{-/-}$ ob/ob mice (*closed squares*), $n = 3$, ob/ob mice treated with rosiglitazone (*open circles*) and *apoE*$^{-/-}$ ob/ob mice treated with rosiglitazone (*open squares*)). *, $p < 0.05$, **, $p < 0.01$.

apoE-deficient ob/ob mice was significantly increased by treatment with rosiglitazone as compared with treatment with the vehicle (Fig. 6*B*).

It has recently been reported that chronic inflammation and oxidative stress in WAT play a crucial role in the development of obesity-related insulin resistance (35–37). Moreover, it has been shown that rosiglitazone suppresses the expression of inflammatory genes in WAT of ob/ob mice (37). To investigate the mechanism by which rosiglitazone ameliorates insulin resistance in apoE-deficient ob/ob mice without preventing adipocyte hypertrophy, we investigated the effects of rosiglitazone on the expression of inflammatory gene and antioxidant enzyme gene in WAT of apoE-deficient ob/ob mice. The expression of MCP-1 was significantly increased in WAT of apoE-deficient ob/ob mice as compared with that in WAT of the wild-type mice (Fig. 6*D*). Rosiglitazone significantly suppressed the expression of MCP-1 in WAT of apoE-deficient ob/ob mice as compared with the vehicle (Fig. 6*D*). The expression of SOD1 was decreased in apoE-deficient ob/ob mice as compared with that in the wild-type mice (Fig. 6*E*). Rosiglitazone significantly increased the expression of SOD1 in apoE-deficient ob/ob mice as compared with the vehicle (Fig. 6*E*). Taken together, these findings indicate that rosiglitazone may attenuate inflammation and oxidative stress in WAT of apoE-deficient ob/ob mice through the apoE-VLDLR-independent pathway.

Rosiglitazone Does Not Increase Body Weight and WAT Weight in VLDLR-deficient Mice—To further investigate a role for VLDLR in rosiglitazone-induced weight gain, we also examined the effect of rosiglitazone on body weight and WAT weight in VLDLR-deficient mice. Wild-type mice and VLDLR-deficient mice, while on the high fat diet, were treated with rosiglitazone (0.01% food admixture) for 7 weeks. Rosiglitazone significantly increased both body weight and WAT weight in wild-type mice (Fig. 7, *A–D*). In contrast, no significant difference in body weight and WAT weight was observed between rosiglitazone-treated VLDLR-deficient mice and the vehicle-treated VLDLR-deficient mice (Fig. 7, *A–D*). To confirm that rosiglitazone activated PPARγ in WAT of both wild-type mice and VLDLR-deficient mice, we next examined the effect of rosiglitazone on plasma adiponectin concentration and the expression of aP2 and VLDLR in WAT. Plasma adiponectin concentration in both wild-type mice and VLDLR-deficient mice was significantly increased by treatment with rosiglitazone as compared with treatment with the vehicle (Fig.

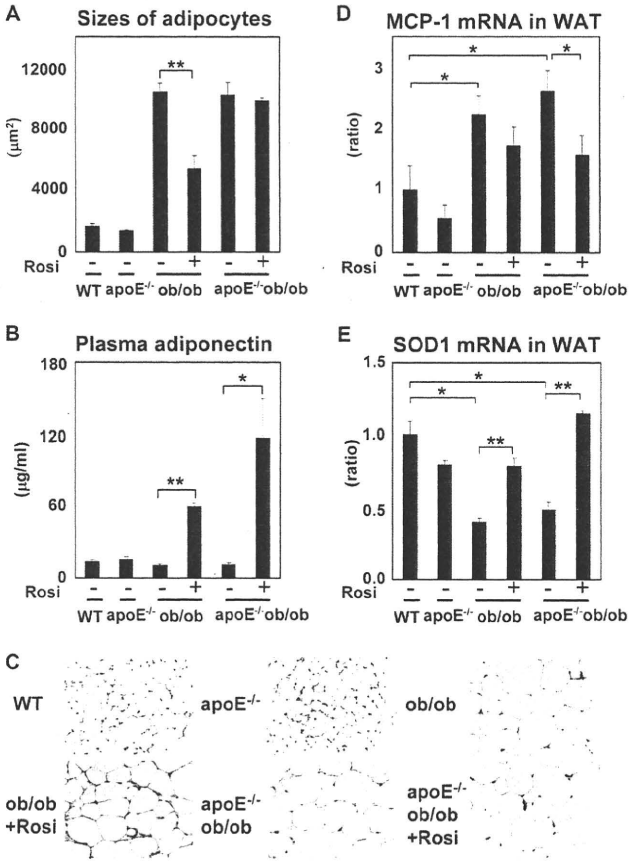

FIGURE 6. **Effects of rosiglitazone treatment for 10 weeks on the size of adipocytes, plasma adiponectin concentration, and gene expression of molecules involved in inflammation and antioxidation in WAT from ob/ob mice and apoE-deficient ob/ob mice.** *A–C*, the size of adipocytes (*A*), plasma adiponectin concentration (*B*), and the section of epididymal WAT (*C*), which were stained with hematoxylin and eosin. WT mice, apoE-deficient mice ($apoE^{-/-}$), ob/ob mice, and apoE-deficient ob/ob mice ($apoE^{-/-}$ob/ob) were fed with the high fat diet for 10 weeks, and ob/ob mice and $apoE^{-/-}$ob/ob mice were treated with 0.01% rosiglitazone (*Rosi*) as food admixture for 10 weeks while on the high fat diet. Each bar represents the means ± S.E. (*error bars*) ($n = 5$, WT mice and $apoE^{-/-}$ mice; $n = 4$, ob/ob mice, ob/ob mice treated with rosiglitazone and $apoE^{-/-}$ob/ob mice; $n = 3$, $apoE^{-/-}$ob/ob mice treated with rosiglitazone). *D* and *E*, amounts of mRNAs of MCP-1 (*D*) and SOD1 (*E*) in epididymal WAT. The mRNA levels of molecules indicated above were quantified by a real-time PCR method as described under "Experimental Procedures." The relative amount of each transcript was normalized to the amount of 36B4 transcript in the same cDNA. The results are expressed as the ratio of the value of WT mice. Each bar represents the means ± S.E. (*error bars*, $n = 3$). *, $p < 0.05$, **, $p < 0.01$.

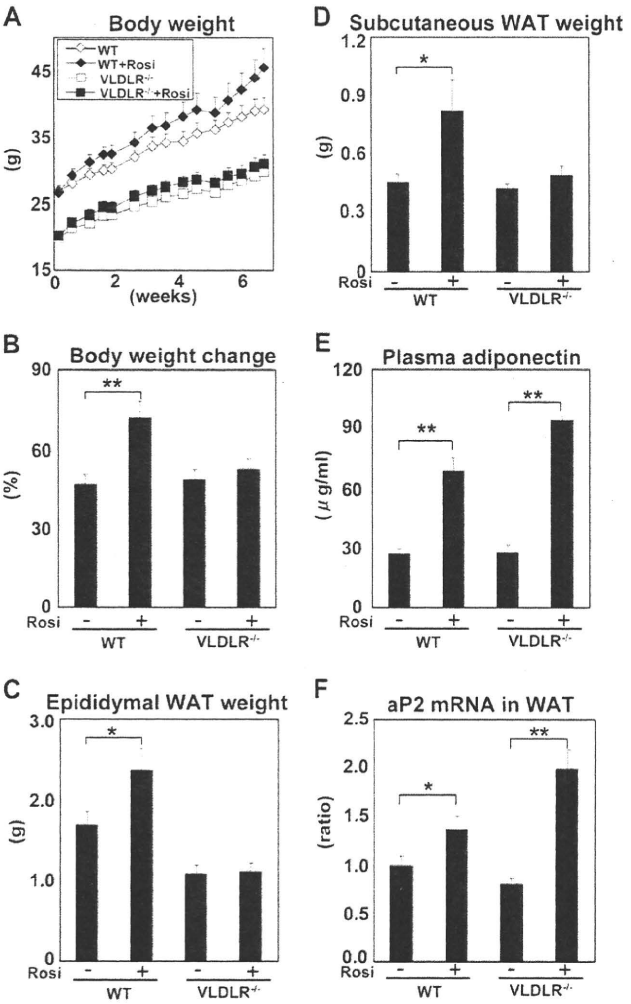

FIGURE 7. **Effects of rosiglitazone treatment for 7 weeks on body weight, WAT weight, plasma adiponectin concentration, and gene expression of aP2 in WAT from wild-type mice and VLDLR-deficient mice.** *A–F*, body weight (*A*), body weight change (*B*), epididymal WAT weight (*C*), subcutaneous WAT weight (*D*), plasma adiponectin concentration (*E*), and amounts of aP2 mRNA (*F*). WT mice and VLDLR-deficient mice ($VLDLR^{-/-}$) were fed with the high fat diet for 7 weeks, and WT mice and $VLDLR^{-/-}$ mice were treated with 0.01% rosiglitazone (*Rosi*) as food admixture for 7 weeks while on the high fat diet. Each bar represents the means ± S.E. (*error bars*) ($n = 7$, WT mice and WT mice treated with rosiglitazone; $n = 5$, $VLDLR^{-/-}$ mice and $VLDLR^{-/-}$ mice treated with rosiglitazone). The percentage of weight change was calculated as final weight minus initial weight divided by initial weight multiplied by 100. *, $p < 0.05$, **, $p < 0.01$.

7*E*). In addition, the expression of aP2 in WAT was also increased by treatment with rosiglitazone in both wild-type mice and VLDLR-deficient mice (Fig. 7*F*). Furthermore, in wild-type mice, rosiglitazone significantly increased the expression of VLDLR in WAT by 1.6-fold as compared with the vehicle (data not shown). These results indicate that VLDLR-mediated lipid uptake into adipocytes plays an important role in rosiglitazone-induced lipid accumulation in adipocytes.

DISCUSSION

TZDs activate PPARγ, which regulates the transcription of genes involved in fatty acid metabolism and storage (15–17). The weight gain associated with TZDs treatment is likely to be due to an increase of lipid accumulation in adipose tissue (28, 29). Recent studies have revealed that apoE-VLDLR interaction plays an important role in the development of obesity and excess fat accumulation (1, 2). However, it remains unclear whether VLDLR-mediated lipid accumulation plays an important role in the weight gain associated with TZD treatment. In this study, we demonstrated that rosiglitazone increases the expression of VLDLR both in WAT *in vivo* and in cultured adipocytes (Figs. 1*A* and 2*A*). Moreover, the use of VLDLR promoter reporter constructs in 3T3-L1 adipocytes led us to identify functional PPRE in the promoter region (Fig. 3, *A–D*). Mutagenesis analyses, EMSA, and the ChIP assay also demonstrated that endogenous PPARγ directly binds to this func-

tional PPRE in the VLDLR promoter region (Fig. 3, *A–F*). These results clearly show that rosiglitazone directly regulates transcription of the VLDLR gene in adipocytes.

To clarify the association between rosiglitazone-induced weight gain and apoE-containing VLDL uptake through VLDLR, we investigated the effects of rosiglitazone on body weight and WAT weight in both apoE-deficient ob/ob mice and VLDLR-deficient mice. In our experiments, rosiglitazone did not increase body weight and WAT weight in apoE-deficient ob/ob mice and VLDLR-deficient mice, but it significantly increased these two parameters in their wild-type control mice (Figs. 4, *A–C*, and 7, *A–D*). It has been shown that apoE deficiency in genetically obese *Ay* mice prevents the development of obesity and that this phenotype is reversed by adenoviral apoE replenishment (2). In addition, it has been reported that VLDLR-deficient mice do not show body weight gain when fed a high fat, high calorie diet (13, 14). Our results in the present study as well as those of previous reports (2, 13, 14) indicate that induction of lipid uptake by rosiglitazone in adipocytes might not work in VLDLR-deficient mice and apoE-deficient ob/ob mice because of lack of the apoE-VLDLR pathway. It is therefore suggested that the apoE-VLDLR pathway plays a crucial role in rosiglitazone-induced lipid accumulation in adipose tissue. Because our results do not exclude the possibility that other receptors contribute to the uptake of VLDL particles into adipocytes, further studies are needed to elucidate the extent to which the apoE-VLDLR pathway is responsible for rosiglitazone-induced lipid uptake.

We also investigated in this study the mechanism by which rosiglitazone ameliorates insulin resistance in apoE-deficient ob/ob mice without affecting WAT weight. It has been reported that rosiglitazone increases the number of small adipocytes and plasma adiponectin concentration, thereby ameliorating insulin resistance (26, 31, 33). Although there was no significant difference in the size of adipocytes in WAT between the vehicle- and rosiglitazone-treated apoE-deficient ob/ob mice, plasma adiponectin concentration was increased by treatment with rosiglitazone (Fig. 6*B*). These results suggest that, in addition to the increase in the number of small adipocytes, the increase in plasma adiponectin levels considerably contributes to the insulin-sensitizing action of TZDs. Furthermore, it has been reported that obesity-associated metabolic syndrome leads to increase in oxidative stress and macrophages accumulation in WAT, which are causes of adipocytes dysfunction (35–37). In the present study, rosiglitazone increased the expression of antioxidant enzyme and reduced the expression of macrophage-specific gene in WAT, suggesting the reduction of oxidative stress and inflammation in WAT (Fig. 6, *D* and *E*). Thus, normalization of adipocyte function might be another possible mechanism by which rosiglitazone improves glucose intolerance and insulin resistance in apoE-deficient ob/ob mice.

In conclusion, we demonstrated in this study that PPARγ directly binds to the functional PPRE in the VLDLR promoter region and that the PPARγ agonist rosiglitazone increases VLDLR expression, which may be involved in lipid accumulation in WAT. We therefore propose that VLDLR-mediated apoE-containing VLDL uptake plays an important role in lipid accumulation induced by rosiglitazone in adipocytes.

Acknowledgments—We are grateful to A. Okano, A. Itoh, and K. Miyata for excellent technical assistance.

REFERENCES

1. Chiba, T., Nakazawa, T., Yui, K., Kaneko, E., and Shimokado, K. (2003) *Arterioscler. Thromb. Vasc. Biol.* **23,** 1423–1429
2. Gao, J., Katagiri, H., Ishigaki, Y., Yamada, T., Ogihara, T., Imai, J., Uno, K., Hasegawa, Y., Kanzaki, M., Yamamoto, T. T., Ishibashi, S., and Oka, Y. (2007) *Diabetes* **56,** 24–33
3. Kraft, H. G., Menzel, H. J., Hoppichler, F., Vogel, W., and Utermann, G. (1989) *J. Clin. Invest.* **83,** 137–142
4. Zechner, R., Moser, R., Newman, T. C., Fried, S. K., and Breslow, J. L. (1991) *J. Biol. Chem.* **266,** 10583–10588
5. Breslow, J. L. (1985) *Annu. Rev. Biochem.* **54,** 699–727
6. Hussain, M. M., Maxfield, F. R., Más-Oliva, J., Tabas, I., Ji, Z. S., Innerarity, T. L., and Mahley, R. W. (1991) *J. Biol. Chem.* **266,** 13936–13940
7. Gåfvels, M. E., Paavola, L. G., Boyd, C. O., Nolan, P. M., Wittmaack, F., Chawla, A., Lazar, M. A., Bucan, M., Angelin, B. O., and Strauss, J. F., 3rd (1994) *Endocrinology* **135,** 387–394
8. Goudriaan, J. R., Espirito, Santo, S. M., Voshol, P. J., Teusink, B., van Dijk, K. W., van Vlijmen, B. J., Romijn, J. A., Havekes, L. M., and Rensen, P. C. (2004) *J. Lipid Res.* **45,** 1475–1481
9. Sakai, J., Hoshino, A., Takahashi, S., Miura, Y., Ishii, H., Suzuki, H., Kawarabayasi, Y., and Yamamoto, T. (1994) *J. Biol. Chem.* **269,** 2173–2182
10. Takahashi, S., Kawarabayasi, Y., Nakai, T., Sakai, J., and Yamamoto, T. (1992) *Proc. Natl. Acad. Sci. U.S.A.* **89,** 9252–9256
11. Takahashi, S., Suzuki, J., Kohno, M., Oida, K., Tamai, T., Miyabo, S., Yamamoto, T., and Nakai, T. (1995) *J. Biol. Chem.* **270,** 15747–15754
12. Zenimaru, Y., Takahashi, S., Takahashi, M., Yamada, K., Iwasaki, T., Hattori, H., Imagawa, M., Ueno, M., Suzuki, J., and Miyamori, I. (2008) *Biochem. Biophys. Res. Commun.* **368,** 716–722
13. Yagyu, H., Lutz, E. P., Kako, Y., Marks, S., Hu, Y., Choi, S. Y., Bensadoun, A., and Goldberg, I. J. (2002) *J. Biol. Chem.* **277,** 10037–10043
14. Goudriaan, J. R., Tacken, P. J., Dahlmans, V. E., Gijbels, M. J., van Dijk, K. W., Havekes, L. M., and Jong, M. C. (2001) *Arterioscler. Thromb. Vasc. Biol.* **21,** 1488–1493
15. Auwerx, J. (1999) *Diabetologia* **42,** 1033–1049
16. Kersten, S., Desvergne, B., and Wahli, W. (2000) *Nature* **405,** 421–424
17. Spiegelman, B. M., and Flier, J. S. (1996) *Cell* **87,** 377–389
18. Chawla, A., Schwarz, E. J., Dimaculangan, D. D., and Lazar, M. A. (1994) *Endocrinology* **135,** 798–800
19. Lowell, B. B. (1999) *Cell* **99,** 239–242
20. Tontonoz, P., Hu, E., and Spiegelman, B. M. (1994) *Cell* **79,** 1147–1156
21. Sato, O., Kuriki, C., Fukui, Y., and Motojima, K. (2002) *J. Biol. Chem.* **277,** 15703–15711
22. Lehmann, J. M., Moore, L. B., Smith-Oliver, T. A., Wilkison, W. O., Willson, T. M., and Kliewer, S. A. (1995) *J. Biol. Chem.* **270,** 12953–12956
23. Way, J. M., Harrington, W. W., Brown, K. K., Gottschalk, W. K., Sundseth, S. S., Mansfield, T. A., Ramachandran, R. K., Willson, T. M., and Kliewer, S. A. (2001) *Endocrinology* **142,** 1269–1277
24. Chao, L., Marcus-Samuels, B., Mason, M. M., Moitra, J., Vinson, C., Arioglu, E., Gavrilova, O., and Reitman, M. L. (2000) *J. Clin. Invest.* **106,** 1221–1228
25. de Souza, C. J., Eckhardt, M., Gagen, K., Dong, M., Chen, W., Laurent, D., and Burkey, B. F. (2001) *Diabetes* **50,** 1863–1871
26. Yamauchi, T., Kamon, J., Waki, H., Terauchi, Y., Kubota, N., Hara, K., Mori, Y., Ide, T., Murakami, K., Tsuboyama-Kasaoka, N., Ezaki, O., Akanuma, Y., Gavrilova, O., Vinson, C., Reitman, M. L., Kagechika, H., Shudo, K., Yoda, M., Nakano, Y., Tobe, K., Nagai, R., Kimura, S., Tomita, M., Froguel, P., and Kadowaki, T. (2001) *Nat. Med.* **7,** 941–946
27. Yamauchi, T., Kamon, J., Waki, H., Imai, Y., Shimozawa, N., Hioki, K., Uchida, S., Ito, Y., Takakuwa, K., Matsui, J., Takata, M., Eto, K., Terauchi, Y., Komeda, K., Tsunoda, M., Murakami, K., Ohnishi, Y., Naitoh, T., Yamamura, K., Ueyama, Y., Froguel, P., Kimura, S., Nagai, R., and Kadowaki, T. (2003) *J. Biol. Chem.* **278,** 2461–2468
28. Kubota, N., Terauchi, Y., Yamauchi, T., Kubota, T., Moroi, M., Matsui, J.,

Eto, K., Yamashita, T., Kamon, J., Satoh, H., Yano, W., Froguel, P., Nagai, R., Kimura, S., Kadowaki, T., and Noda, T. (2002) *J. Biol. Chem.* **277,** 25863–25866
29. Moore, G. B., Chapman, H., Holder, J. C., Lister, C. A., Piercy, V., Smith, S. A., and Clapham, J. C. (2001) *Biochem. Biophys. Res. Commun.* **286,** 735–741
30. Yamauchi, T., Kamon, J., Waki, H., Murakami, K., Motojima, K., Komeda, K., Ide, T., Kubota, N., Terauchi, Y., Tobe, K., Miki, H., Tsuchida, A., Akanuma, Y., Nagai, R., Kimura, S., and Kadowaki, T. (2001) *J. Biol. Chem.* **276,** 41245–41254
31. Yamauchi, T., Waki, H., Kamon, J., Murakami, K., Motojima, K., Komeda, K., Miki, H., Kubota, N., Terauchi, Y., Tsuchida, A., Tsuboyama-Kasaoka, N., Yamauchi, N., Ide, T., Hori, W., Kato, S., Fukayama, M., Akanuma, Y., Ezaki, O., Itai, A., Nagai, R., Kimura, S., Tobe, K., Kagechika, H., Shudo, K., and Kadowaki, T. (2001) *J. Clin. Invest.* **108,** 1001–1013
32. Yamauchi, T., Kamon, J., Ito, Y., Tsuchida, A., Yokomizo, T., Kita, S., Sugiyama, T., Miyagishi, M., Hara, K., Tsunoda, M., Murakami, K., Ohteki, T., Uchida, S., Takekawa, S., Waki, H., Tsuno, N. H., Shibata, Y., Terauchi, Y., Froguel, P., Tobe, K., Koyasu, S., Taira, K., Kitamura, T., Shimizu, T., Nagai, R., and Kadowaki, T. (2003) *Nature* **423,** 762–769
33. Okuno, A., Tamemoto, H., Tobe, K., Ueki, K., Mori, Y., Iwamoto, K., Umesono, K., Akanuma, Y., Fujiwara, T., Horikoshi, H., Yazaki, Y., and Kadowaki, T. (1998) *J. Clin. Invest.* **101,** 1354–1361
34. Tsuchida, A., Yamauchi, T., Takekawa, S., Hada, Y., Ito, Y., Maki, T., and Kadowaki, T. (2005) *Diabetes* **54,** 3358–3370
35. Weisberg, S. P., McCann, D., Desai, M., Rosenbaum, M., Leibel, R. L., and Ferrante, A. W., Jr. (2003) *J. Clin. Invest.* **112,** 1796–1808
36. Xu, H., Barnes, G. T., Yang, Q., Tan, G., Yang, D., Chou, C. J., Sole, J., Nichols, A., Ross, J. S., Tartaglia, L. A., and Chen, H. (2003) *J. Clin. Invest.* **112,** 1821–1830
37. Furukawa, S., Fujita, T., Shimabukuro, M., Iwaki, M., Yamada, Y., Nakajima, Y., Nakayama, O., Makishima, M., Matsuda, M., and Shimomura, I. (2004) *J. Clin. Invest.* **114,** 1752–1761

nature medicine

$CD8^+$ effector T cells contribute to macrophage recruitment and adipose tissue inflammation in obesity

Satoshi Nishimura[1–4], Ichiro Manabe[1,2,4,5], Mika Nagasaki[1,6], Koji Eto[7], Hiroshi Yamashita[1], Mitsuru Ohsugi[8], Makoto Otsu[7], Kazuo Hara[8], Kohjiro Ueki[3,5,8], Seiryo Sugiura[9], Kotaro Yoshimura[10], Takashi Kadowaki[3,5,8] & Ryozo Nagai[1,3,5]

Inflammation is increasingly regarded as a key process underlying metabolic diseases in obese individuals. In particular, obese adipose tissue shows features characteristic of active local inflammation. At present, however, little is known about the sequence of events that comprises the inflammatory cascade or the mechanism by which inflammation develops. We found that large numbers of $CD8^+$ effector T cells infiltrated obese epididymal adipose tissue in mice fed a high-fat diet, whereas the numbers of $CD4^+$ helper and regulatory T cells were diminished. The infiltration by $CD8^+$ T cells preceded the accumulation of macrophages, and immunological and genetic depletion of $CD8^+$ T cells lowered macrophage infiltration and adipose tissue inflammation and ameliorated systemic insulin resistance. Conversely, adoptive transfer of $CD8^+$ T cells to CD8-deficient mice aggravated adipose inflammation. Coculture and other *in vitro* experiments revealed a vicious cycle of interactions between $CD8^+$ T cells, macrophages and adipose tissue. Our findings suggest that obese adipose tissue activates $CD8^+$ T cells, which, in turn, promote the recruitment and activation of macrophages in this tissue. These results support the notion that $CD8^+$ T cells have an essential role in the initiation and propagation of adipose inflammation.

Inflammation is now considered to have a pivotal role in the development of metabolic diseases[1]. In particular, obese adipose tissue shows the hallmarks of chronic inflammation[2,3], and the inflammation is thought to alter adipose tissue function, leading to systemic insulin resistance[4]. The mechanism by which the development of this insulin resistance occurs is believed to involve proinflammatory cytokines produced by infiltrating macrophages and resident adipocytes within the obese adipose tissue[1]. Likewise, chronic inflammation also impairs triglyceride storage in adipose tissues, and the excess circulating free fatty acids and triglycerides also induces insulin resistance in muscle and liver[5–7]. Adding insult to injury, it has been postulated that a paracrine loop involving these free fatty acids and inflammatory cytokines establishes a vicious cycle that aggravates the inflammatory changes, furthering the dysfunction of adipose tissue[8]. As such, the inflammatory changes seen in obese adipose tissue may be the key pathology that promotes systemic inflammatory states and insulin resistance in obese individuals.

Macrophage infiltration of adipose tissue has been described in both mice and humans[1]. However, little is known about the sequence of events that lead to macrophage infiltration. Recently accumulation of other immune cells, such as T cells, has been documented in obese adipose tissue[9,10]. T lymphocytes are known to interact with macrophages and regulate the inflammatory cascade[11]. However, their functional role in adipose inflammation remains unclear. Here we show that infiltration of $CD8^+$ effector T cells is an early event during the development of adipose tissue obesity induced by a high-fat diet. Further, we show using loss- and gain-of-function approaches *in vivo* that these T cells are critical mediators of systemic metabolic dysfunction. Finally, we also show *in vitro* that obese adipose tissue can activate $CD8^+$ T cells, which, in turn, allows for the recruitment and differentiation of macrophages. Thus, together our findings indicate that $CD8^+$ T cells have essential roles in the initiation and maintenance of adipose tissue inflammation and systemic insulin resistance. Our results also clearly show the involvement of adaptive immunity in metabolic disorders.

RESULTS

$CD8^+$ T cell infiltration precedes macrophage accumulation

Adipose tissue consists of not only adipocytes but also stromal and vascular cells, including fibroblasts, vascular endothelial cells and inflammatory cells. This stromal vascular fraction is known to be essential for adipose tissue inflammation[2]. Therefore, to gain insight

[1]Department of Cardiovascular Medicine, [2]Nano-Bioengineering Education Program and [3]Translational Systems Biology and Medicine Initiative, Graduate School of Medicine, The University of Tokyo, Tokyo, Japan. [4]PRESTO, Japan Science and Technology Agency, Kawaguchi, Japan. [5]Comprehensive Center of Education and Research for Chemical Biology of the Diseases, [6]Computational Diagnostic Radiology and Preventive Medicine, The University of Tokyo, Tokyo, Japan. [7]Division of Stem Cell Therapy, Center for Stem Cell Biology and Regenerative Medicine, Institute of Medical Science, The University of Tokyo, Tokyo, Japan. [8]Department of Metabolic Diseases, Graduate School of Medicine, The University of Tokyo, Tokyo, Japan. [9]Department of Human and Engineered Environmental Studies, Graduate School of Frontier Sciences, The University of Tokyo, Tokyo, Japan. [10]Department of Plastic Surgery, Graduate School of Medicine, The University of Tokyo, Tokyo, Japan. Correspondence should be addressed to S.N. (snishi-tky@umin.ac.jp) or I.M. (manabe-tky@umin.ac.jp).

Received 5 January; accepted 7 April; published online 26 July 2009; doi:10.1038/nm.1964

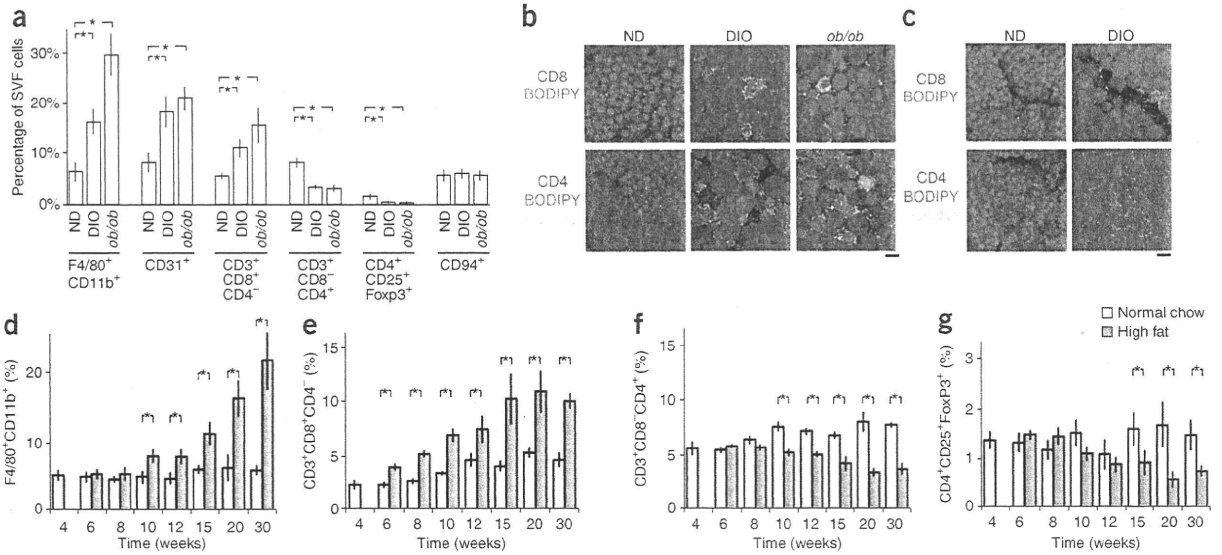

Figure 1 Differential infiltration of lymphocytes and macrophages into obese adipose tissue. (**a**) Flow cytometric analysis of the stromal vascular fraction (SVF) from the epididymal fat pads of control mice fed a normal chow diet (ND), diet-induced obese (DIO) mice fed a high-fat diet for 16 weeks and *ob/ob* mice fed a normal diet (*ob/ob*). All mice were 20-weeks-old. The cell populations of macrophages ($F4/80^+CD11b^+$), endothelial cells ($CD31^+$), $CD3^+CD8^+CD4^-$ T cells, $CD3^+CD8^-CD4^+$ T cells, regulatory T cells ($CD4^+CD25^+Foxp3^+$) and NK cells ($CD3^-CD94^+$) were analyzed ($n = 5$ mice in each group). The number of each cell type was normalized to the total number of viable SVF cells. $^*P < 0.05$. (**b**,**c**) Immunohistochemical analysis of CD8 and CD4 (each in red) in epididymal (**b**) and femoral subcutaneous (**c**) adipose tissue from ND, DIO and *ob/ob* mice. Adipocytes were counterstained with boron-dipyrromethene (BODIPY, blue) and nuclei with Hoechst (green). Quantification of $CD8^+$ and $CD4^+$ cells is shown in **Supplementary Fig. 3**. Scale bars, 100 μm. (**d**–**g**) Time courses of changes in the cell populations in the adipose stroma during development of obesity. Flow cytometric analysis of the stromal vascular fraction from the epididymal fat pads of control mice fed a normal chow diet and mice fed a high-fat diet beginning when they were 4-weeks-old. Numbers of macrophages (**d**), $CD8^+$ T cells (**e**), $CD4^+$ T cells (**f**) and regulatory T cells (**g**) were determined during the course of DIO development ($n = 5$ mice in each group; $^*P < 0.05$). Error bars represent means ± s.e.m.

into the inflammatory processes taking place within these cell fractions during obesity, we first analyzed immune cell populations in collagenase-digested stromal vascular fractions from obese epididymal adipose tissue with the aim of identifying local obesity-induced immunological changes. We acquired stromal vascular fractions using previously described methods of isolation[12] with a few modifications. We first carried out a set of flow cytometric analyses to determine the proper gating for analysis of lymphocytes and macrophages in adipose tissue (**Supplementary Fig. 1**). We found that R1 gating accounted for the majority of viable cells, including a majority of $F4/80^+CD11b^+$ macrophages. Because earlier studies used broader gating to analyze macrophages in the stromal vascular fraction[13], we compared the broader R2 gating with the narrower R1 gating. We found that the macrophage and lymphocyte fractions detected with R1 gating did not significantly differ from those detected using the broader R2 gating (**Supplementary Fig. 1** and **Supplementary Table 1**). For that reason, we analyzed subsequent cell fractions by R1 gating (for further discussion of gating, see **Supplementary Methods** and **Supplementary Fig. 1**).

Consistent with earlier reports[2], the infiltration of $F4/80^+CD11b^+$ macrophages into adipose tissue was significantly increased by diet-induced obesity (DIO) and in obese *ob/ob* mice compared to the control lean mice on a normal diet ($P < 0.05$) (**Fig. 1a**). The numbers of $CD31^+$ endothelial cells were also higher in obese mice (**Fig. 1a**), which may reflect angiogenesis[14]. Notably, we found that $CD3^+$ T cells accounted for 14.8 ± 0.9% of stromal vascular cells in lean adipose tissue, and most (94.7 ± 0.3%) of the $CD3^+$ T cells were CD4 or CD8 positive. The $CD3^+CD8^+CD4^-$ T cell fraction was larger in obese adipose tissue, whereas the $CD3^+CD4^+CD8^-$ T cell fraction was smaller, as was the regulatory T cell fraction ($CD4^+CD25^+Foxp3^+$) compared to lean mice on normal diet ($P < 0.05$). The natural killer (NK) cell fraction ($CD3^-CD94^+$) was unaffected by obesity (**Fig. 1a**). In contrast to the higher number of $CD8^+$ lymphocytes seen in obese adipose tissue, $CD8^+$ and $CD4^+$ T cell counts were significantly lower in peripheral blood from *ob/ob* mice and were unchanged in DIO mice as compared to mice on a normal diet ($P < 0.05$) (**Supplementary Fig. 2**), suggesting selective recruitment of $CD8^+$ T lymphocytes to obese adipose tissues.

Immunohistochemical analysis of F4/80, CD8 and CD4 expression also revealed higher numbers of $F4/80^+$ macrophages and $CD8^+$ T cells and lower numbers of $CD4^+$ T cells in obese epididymal fat pads as compared to mice on a normal diet ($P < 0.05$) (**Fig. 1b** and **Supplementary Fig. 3**). By contrast, we found no significant changes in the numbers of $CD8^+$ and $CD4^+$ cells in subcutaneous fat pads (**Fig. 1c**). In obese epididymal adipose tissues, we found a number of $CD8^+$ cells within 'crown-like structures' (CLSs), which reflect the focal convergence of macrophages surrounding necrotic adipocytes[14,15] (**Fig. 1b**), whereas $CD4^+$ cells showed no apparent relationship with CLSs.

Most $CD3^+CD8^+$ cells were $CD62L^-$ and $CD44^+$ (74.7% ± 3.8% of $CD3^+$ $CD8^+$ cells in DIO mice), suggesting the majority of infiltrated $CD8^+$ T cells were activated effector T cells[16]. To assess the clonality of $CD8^+$ in obese adipose, we examined the T cell receptor (TCR) V_β repertoire of $CD8^+$ T cells in lean and obese adipose tissues. The results showed that $CD8^+$ T cells in obese adipose were not monoclonal, though the $CD8^+$ cell fractions that were positive for $V_{\beta 7}$ and $V_{\beta 20b}$ were significantly larger in obese adipose tissues as compared to mice on a normal diet ($P < 0.05$) (**Supplementary Fig. 4**).

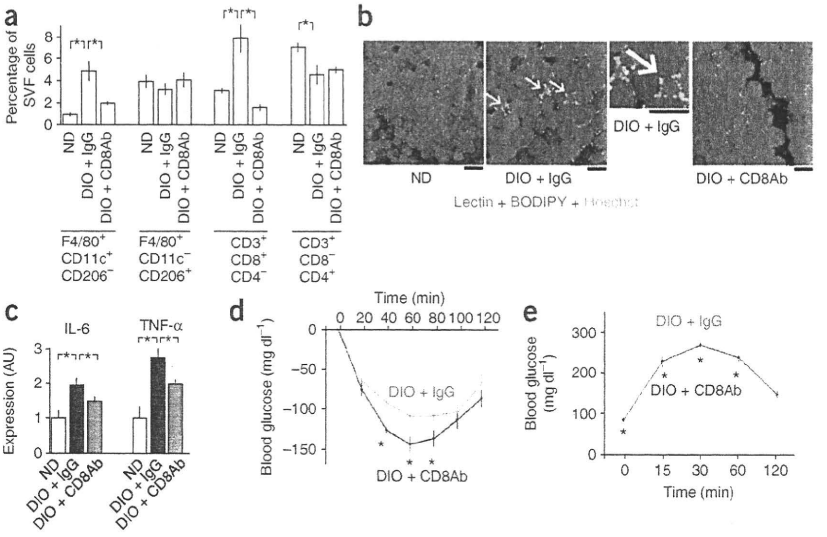

Figure 2 Effects of CD8-specific antibody treatment on obese adipose tissue inflammation. (**a**) Flow cytometric analysis of M1 macrophages ($F4/80^+CD11c^+CD206^-$), M2 macrophages ($F4/80^+CD11c^-CD206^+$), $CD8^+$ T cells and $CD4^+$ T cells in stromal vascular fractions in mice from lean normal-diet (ND), and DIO mice administered either antibody to CD8 (DIO + CD8Ab) or control IgG (DIO + IgG). The same mice were used in **b**–**e**. High-fat diet was started at the age of 4-weeks-old, and all of the mice were examined at 12-weeks-old. ($n = 5$ mice in each group). (**b**) Histochemical identification of endothelial cells (lectin, red), adipocytes (BODIPY, blue) and nuclei (Hoechst, green) in epididymal adipose tissue. White arrows indicate CLSs. Scale bars, 100 μm. (**c**) Real-time PCR analysis of cytokine expression in adipose tissue. The levels of each transcript were normalized to that in the lean control ($n = 5$ mice in each group). AU, arbitrary units. (**d**,**e**) Results of insulin tolerance (**d**, 0.75 U insulin per kg body weight) and oral glucose tolerance (**e**, 1 g per kg glucose) tests in DIO mice treated with antibody to CD8 or control IgG ($n = 8$ mice in each group). $^*P < 0.05$. Error bars represent means ± s.e.m.

It is known that one consequence of macrophage accumulation, particularly M1 macrophages, in inflamed adipose tissue is modulation and impairment of the tissue's function[17]. It is not known, however, what initiates macrophage infiltration or the resultant inflammatory cascade. The dynamic changes in lymphocyte populations seen in obese adipose tissue (**Fig. 1a,b**) suggest that lymphocytes might have a key role. To test this idea, we examined the time course of changes in stromal cell populations during the progression of DIO. We fed C57BL/6 mice a high-fat diet, beginning when they were 4-weeks-old (**Fig. 1d–g**). Within 2 weeks, the $CD8^+CD4^-$ T cell fraction within the total stromal vascular cell fraction was significantly increased in the stroma of the epididymal fat, as compared to that in mice fed a control chow diet (**Fig. 1e**). The numbers of $CD8^+CD4^-$ T cells continued to increase thereafter, peaking when the mice were 15-weeks-old (**Fig. 1e**). By contrast, the fractions of $CD8^-CD4^+$ T cells and $CD4^+CD25^+FoxP3^+$ regulatory T cells were reduced at later times (**Fig. 1f,g**), suggesting that $CD8^+$ T cell infiltration is a primary event during inflammatory cascades within adipose tissue. The increase in $CD8^+$ T cells also preceded the accumulation of macrophages when cell numbers were expressed per fat pad (**Supplementary Fig. 5**), clearly indicating that $CD8^+$ cells infiltrated into the epididymal fat pads of DIO mice before macrophage infiltration.

To gain additional insight into the clinical importance of $CD8^+$ T cells in obese fat, we analyzed the expression of *CD8A* in samples of human subcutaneous adipose tissue. Levels of *CD8A* expression were significantly higher in obese subjects than in lean ones ($P < 0.05$), suggesting that $CD8^+$ T cells also accumulate in human obese adipose tissue (**Supplementary Fig. 6**).

CD8 depletion inhibits inflammatory cascade in obese adipose

To assess the role of $CD8^+$ T cells in adipose inflammation, we examined the effects of CD8 depletion using neutralizing antibody treatment on the inflammatory response in obese adipose tissue. We randomly assigned male C57BL/6 mice to two groups and intraperitoneally administered either antibody to CD8 or control IgG once a week for 8 weeks, beginning when the mice were 4-weeks-old. We fed the mice a high-fat diet over the same period, and we performed metabolic and histological analyses at 12 weeks of age. Antibody to CD8 treatment had no effect on body weight, food intake, fat pad weight or adipocyte diameter (**Supplementary Fig. 7**). However, it significantly lowered the $CD8^+CD4^-$ T cell fraction in the epididymal fat pads without affecting the $CD8^-CD4^+$ cell fraction (**Fig. 2a**). It also reduced the infiltrated M1 macrophage ($F4/80^+CD11c^+CD206^-$) fraction without affecting the M2 macrophage ($F4/80^+CD11c^-CD206^+$) fraction[17] and significantly lowered the numbers of CLSs ($P < 0.05$ for each) (**Fig. 2b** and **Supplementary Fig. 7d**).

The messenger RNA expression of the proinflammatory cytokines interleukin-6 (IL-6) and tumor necrosis factor-α (TNF-α) in epididymal fat pads was lowered by CD8-specific antibody treatment (**Fig. 2c**), as were their serum concentrations (**Supplementary Fig. 7f**). In addition, the insulin resistance and glucose intolerance induced by the high-fat diet were ameliorated by CD8-specific antibody treatment (**Fig. 2d,e**). Similarly, CD8-specific antibody treatment lowered M1 macrophage infiltration into epididymal fat and ameliorated systemic insulin resistance in *ob/ob* mice (**Supplementary Fig. 8**). Collectively, these effects of CD8-specific antibody treatment clearly show that $CD8^+$ cells are required for the recruitment of macrophages into obese adipose tissue and the initiation and propagation of inflammatory responses there.

CD8 depletion ameliorates pre-established inflammation

We next examined the activity of $CD8^+$ T cells in obese adipose tissues in which inflammation had already been established. We began administering antibodies to 19-week-old DIO mice that had been fed a high-fat diet since they were 9-weeks-old. We intraperitoneally administered either antibody to CD8 or control IgG three times per week for 2 weeks, and examined the mice at 21-weeks-old. Treatment with antibody to CD8 suppressed $CD8^+$ T cell infiltration into obese fat pads without affecting $CD4^+$ T cells (**Fig. 3a**). CD8 antibody also lowered M1 ($F4/80^+CD11c^+$) macrophage fraction while leaving the M2 macrophage ($F4/80^+CD11c^-$) fraction unchanged (**Fig. 3a**). The reduction in macrophage infiltration was confirmed by F4/80 immunohistochemistry (**Fig. 3b**). In addition, the number of CLSs was also lowered by CD8-specific antibody treatment (**Fig. 3b,c**). DIO led to upregulated mRNA expression of the proinflammatory cytokines IL-1, IL-6 and TNF-α, as well as of

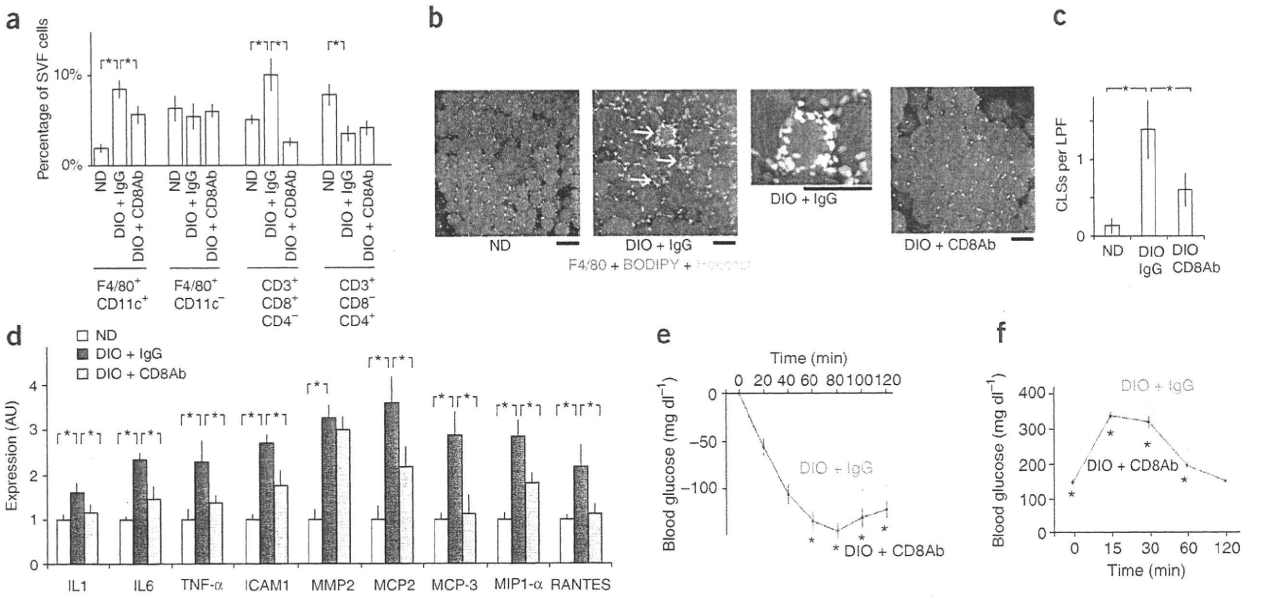

Figure 3 Effects of CD8-specific antibody treatment on pre-established obese adipose inflammation. (**a**) Flow cytometric analysis of cell populations in stromal vascular fractions from control mice on a normal chow diet (ND) and DIO mice administered control IgG (DIO + IgG) or antibody to CD8 (DIO + CD8Ab) three times per week from 19- to 21-weeks-old. ($n = 5$ mice in each group). High-fat diet was started at the age of 9-weeks-old, and all the mice were examined at 21-weeks-old. The same mice were used in **b**–**f**. (**b**) Immunohistochemical identification of macrophages (F4/80, red) in epididymal adipose tissue. Adipocytes were counterstained with BODIPY (blue), and the nuclei with Hoechst (green). Scale bars, 100 μm. (**c**) Numbers of CLSs (shown by white arrows in **b**) in adipose tissue ($n = 20$ low-power fields (LPF) in each group). (**d**) Real-time PCR analysis of cytokine expression in epididymal adipose tissue. The levels of each transcript were normalized to those in control ND mice. MIP, monocyte inflammatory protein ($n = 5$ mice in each group). (**e**,**f**) Results of insulin tolerance (**e**, 1 U insulin per kg body weight) and oral glucose tolerance (**f**, 1 g per kg glucose) tests in DIO mice treated with antibody to CD8 or control IgG ($n = 10$ mice in each group). $^*P < 0.05$. Error bars represent means ± s.e.m.

intercellular adhesion molecule-1 (ICAM1) and matrix metalloproteinase-2 (MMP-2), in adipose tissue, which is consistent with local inflammation, and CD8-specific antibody treatment lowered expression of all of these mediators (**Fig. 3d**).

CD8-specific antibody treatment also ameliorated insulin resistance and glucose intolerance in DIO mice (**Fig. 3e,f** and **Supplementary Fig. 9**). These results clearly show that CD8-specific antibody treatment suppresses preexisting adipose inflammation, which strongly suggests that $CD8^+$ cells are required for the maintenance of inflammatory reactions in obese adipose tissue.

$CD8^+$ T cells are required for adipose tissue inflammation

To further establish the requirement for $CD8^+$ T cells in adipose inflammation *in vivo*, we started 6-week-old genetically CD8-deficient mice on a high-fat diet and maintained them on it for 8 weeks, and examined the $CD8a^{-/-}$ mice at 14-weeks-old. In sharp contrast to wild-type mice fed the same high-fat diet (**Fig. 1**), the CD8-deficient mice did not show significant increases in the M1 or M2 macrophage fraction in the epididymal fat under high-fat diet (**Fig. 4a**), and we found very few CLSs (**Fig. 4b,c**), although both body weight and epididymal fat mass were significantly higher compared to $CD8a^{-/-}$ mice on a normal diet (**Supplementary Fig. 10a,b**). Levels of proinflammatory cytokine mRNA expression in adipose tissue, including IL-6 and TNF-α, also were not increased by the high-fat diet in CD8-deficient mice (**Fig. 4d**).

To directly examine the role of $CD8^+$ T cells in adipose tissue inflammation, we adoptively transferred splenic $CD8^+$ T cells into CD8-deficient mice. We intravenously administered either 5×10^6 splenic $CD8^+$ T cells isolated from 7-week-old C57BL/6 mice or control vehicle weekly over the same period and examined the $CD8a^{-/-}$ mice at 14-weeks-old. Adoptive transfer of $CD8^+$ T cells increased M1 macrophage infiltration (**Fig. 4a**), numbers of CLSs (**Fig. 4b,c**), and expression of IL-6 and TNF-α in epididymal fat (**Fig. 4d**), indicating initiation of adipose inflammation. A high-fat diet induced moderate glucose intolerance in untreated CD8-deficient mice, but we did not observe insulin resistance in insulin tolerance tests (**Fig. 4e,f**). Adoptive $CD8^+$ T cell transfer aggravated the glucose intolerance and induced insulin resistance (**Fig. 4e,f**). Taken together, the results that we obtained with CD8-deficient mice confirm that $CD8^+$ T cells are essential for macrophage recruitment and inflammation in adipose tissue in DIO.

Interplay between macrophages, T cells and adipocytes

We next analyzed the cellular interplay via which inflammation develops in obese adipose tissue. On the basis of the findings of the *in vivo* experiments summarized above, we hypothesized that obese adipose tissue activates $CD8^+$ T cells, which, in turn, recruit and activate macrophages. To test this hypothesis, we first cocultured splenic $CD8^+$ T cells with epididymal fat tissue prepared from lean or obese mice to determine whether obese adipose tissue can activate $CD8^+$ T cells. Whereas obese epididymal fat clearly induced T cell proliferation, lean fat did so only modestly (**Fig. 5a**), indicating that obese adipose tissue can indeed activate $CD8^+$ T cells.

To assess the involvement of $CD8^+$ T cells in monocytes and macrophage differentiation, we cocultured various combinations of peripheral blood $CD11b^{high}$ granulocyte-1 $(Gr\text{-}1)^-CD4^-CD8^-$cells (most of which were monocytes), $CD8^+$ cells prepared from either lean or obese adipose tissue, and lean epididymal adipose tissue. By

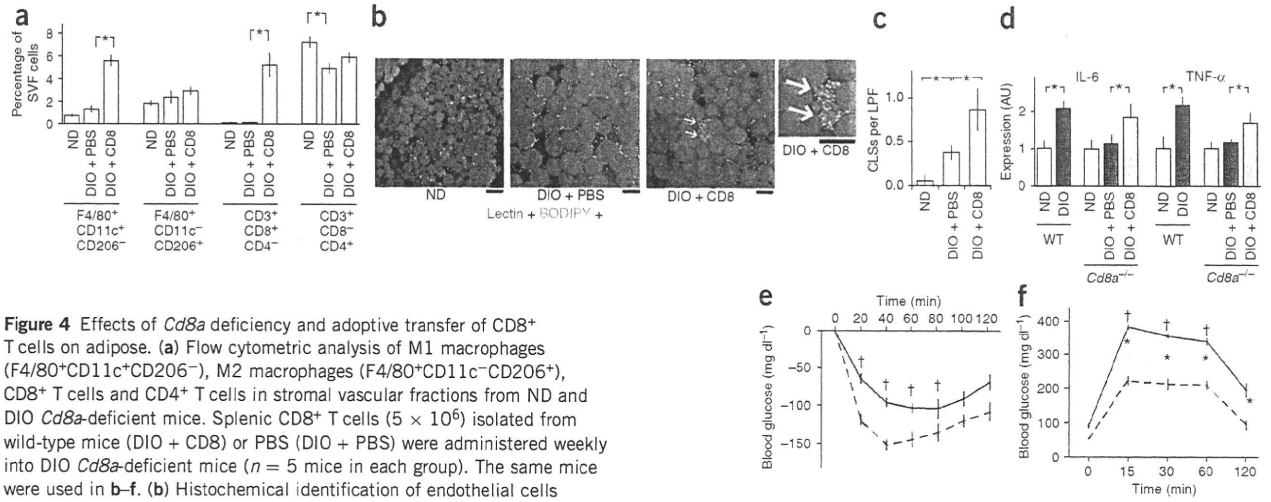

Figure 4 Effects of *Cd8a* deficiency and adoptive transfer of CD8+ T cells on adipose. (**a**) Flow cytometric analysis of M1 macrophages ($F4/80^+CD11c^+CD206^-$), M2 macrophages ($F4/80^+CD11c^-CD206^+$), $CD8^+$ T cells and $CD4^+$ T cells in stromal vascular fractions from ND and DIO *Cd8a*-deficient mice. Splenic $CD8^+$ T cells (5×10^6) isolated from wild-type mice (DIO + CD8) or PBS (DIO + PBS) were administered weekly into DIO *Cd8a*-deficient mice ($n = 5$ mice in each group). The same mice were used in **b–f**. (**b**) Histochemical identification of endothelial cells (lectin, red), adipocytes (BODIPY, blue) and nuclei (Hoechst, green) in epididymal adipose tissue. White arrows indicate CLSs. Scale bars, 100 μm. (**c**) Numbers of CLSs in adipose tissues ($n = 20$ low-power fields in each group). (**d**) Real-time PCR analysis of cytokine expression in adipose tissue from C57BL/6 (WT) ND, WT DIO, and *Cd8a*-deficient ND, DIO + CD8 or DIO + PBS mice. ($n = 5$ mice in each group). $^*P < 0.05$ in **a–d**. (**e**,**f**) Insulin tolerance (**e**, 0.75 U insulin per kg body weight) and oral glucose tolerance (**f**, 1 g per kg) tests of the *Cd8a*-deficient ND (dotted lines), DIO + CD8 and DIO + PBS groups ($n = 6$ mice in each group). $^*P < 0.05$ for ND versus DIO + PBS and $\dagger P < 0.05$ for DIO + PBS versus DIO + CD8. Error bars represent means ± s.e.m.

themselves, neither $CD8^+$ cells nor adipose tissue induced macrophage differentiation (**Fig. 5b**). However, when cocultured with both $CD8^+$ cells and lean adipose tissue, peripheral blood monocytes differentiated into $F4/80^+CD11b^+CD68^+$ macrophages (**Fig. 5b**). Moreover, $CD8^+$ cells from obese adipose tissues generated significantly more macrophages than those from lean adipose (**Fig. 5b**). Thus, $CD8^+$ cells seem to be essential for macrophage differentiation in this setting. Further, the requirement for adipose tissue suggests that the interaction between $CD8^+$ T cells and adipose tissue is necessary for induction of macrophage differentiation.

We then tested whether activated $CD8^+$ cells elicit macrophage migration via humoral interactions. Analysis of the medium conditioned with activated $CD8^+$ T cells showed that these cells secrete substantial amounts of humoral factors known to induce macrophage

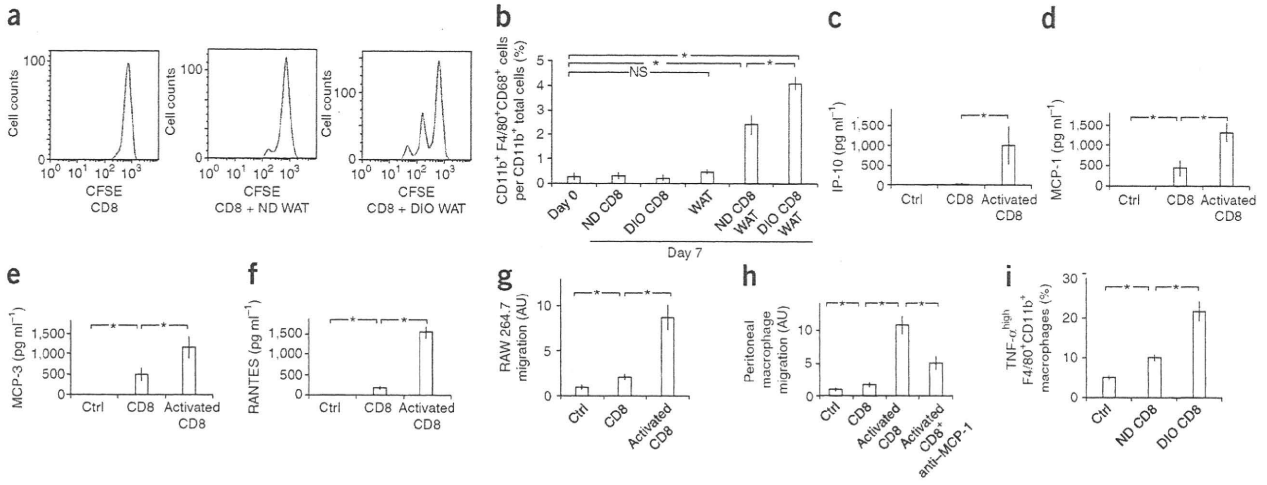

Figure 5 Interplay between macrophages, $CD8^+$ T cells and adipose tissue. (**a**) Carboxyfluorescein succinimidyl ester (CFSE) proliferation assay of isolated splenic $CD8^+$ T cells cultured with or without epididymal adipose tissue from ND or DIO mice. WAT, white adipose tissue. (**b**) Effects of $CD8^+$ T cells and adipose tissue on differentiation of peripheral blood monocytes ($CD11b^{high}Gr\text{-}1^-$) into macrophages ($CD11b^+F4/80^+CD68^+$). Monocytes were cocultured for 7 d with $CD8^+$ T cells isolated from epididymal adipose tissue from lean (ND CD8) or DIO (DIO CD8) mice, with or without epididymal WAT from lean mice. The differentiated macrophage fractions are shown ($n = 5$ in each group; $^*P < 0.05$; NS, not significant). (**c–f**) Concentrations of various cytokines in the control medium and medium conditioned by quiescent (CD8) or activated (activated CD8) CD8 cells ($n = 5$ in each group). $^*P < 0.05$. IP-10, interferon-inducible protein-10. (**g**,**h**) Migration of RAW264.7 (**g**) and peritoneal (**h**) macrophages, as examined using unconditioned control medium (Ctrl), medium conditioned by quiescent (CD8) or activated (activated CD8) $CD8^+$ T cells, or neutralizing antibody to MCP-1 (anti–MCP-1) ($n = 20$ in each group). $^*P < 0.05$. (**i**) The fraction of $F4/80^+$ $CD11b^+$ macrophages producing high levels of TNF-α after isolation from lean epididymal adipose tissue and cultured without (Ctrl) or with $CD8^+$ T cells isolated from ND (ND CD8) or DIO (DIO CD8) mice ($n = 5$ in each group, $^*P < 0.05$). Error bars represent means ± s.e.m.

migration, including interferon-inducible protein-10, monocyte chemoattractant protein-1 (MCP-1), MCP-3 and regulation upon activation, normal T cell expressed and secreted protein (RANTES) (**Fig. 5c–f**). When we plated cells of the macrophage cell line RAW264.7 or isolated peritoneal macrophages in Boyden chambers and treated them with medium conditioned by activated $CD8^+$ T cells, the numbers of both cell types that migrated through the pores between the chamber wells with activated $CD8^+$ T cell–conditioned medium were significantly higher compared to cells cultured in non-conditioned medium ($P < 0.05$ for each) (**Fig. 5g,h**). Treatment with antibody to MCP-1 lowered the migration of peritoneal macrophages by approximately half, indicating MCP-1 to be one of the factors mediating the humoral interactions (**Fig. 5h**).

To further assess the involvement of $CD8^+$ T cells in macrophage activation in adipose tissue, we cocultured $F4/80^+$ $CD11b^+$ macrophages isolated from lean epididymal fat tissue with $CD8^+$ cells isolated from either lean or obese fat tissue. The numbers of macrophages producing high amounts of TNF-α were significantly increased by the $CD8^+$ cells (**Fig. 5i**). Moreover, $CD8^+$ cells from obese adipose tissue increased the number of TNF-α^{high} macrophages to a significantly greater degree than those from lean adipose tissue (**Fig. 5i**). Collectively, then, the results of the coculture experiments show that the interaction between obese adipose tissue and $CD8^+$ T cells is crucial for macrophage differentiation, migration and activation.

DISCUSSION

Adipose tissue inflammation is now considered to be a crucial event leading to the metabolic syndrome, diabetes and atherosclerotic cardiovascular disease. However, it is still unclear how adipose inflammation is initiated and maintained. Here we showed that $CD8^+$ T cell infiltration precedes accumulation of macrophages in adipose tissue obesity, $CD8^+$ T cells are required for adipose tissue inflammation and $CD8^+$ T cells have major roles in macrophage differentiation, activation and migration. Thus, $CD8^+$ T cells are crucially involved in initiating inflammatory cascades in obese adipose tissue. Moreover, the finding that CD8-specific antibody treatment ameliorates preestablished adipose inflammation in DIO mice indicates that $CD8^+$ T cells are also essential for maintenance of the inflammatory response. Although infiltration of T cells into obese adipose tissue has been reported previously[10,18], to our knowledge, the present study is the first to directly address the functional role of $CD8^+$ cells in adipose tissue inflammation. The findings that systemic insulin resistance is ameliorated by CD8 depletion and aggravated by adoptive transfer of $CD8^+$ cells strongly suggest that CD8-dependent adipose inflammation has an impact on systemic metabolism.

Accumulation of $CD8^+$ T cells in obese epididymal fat pads was not accompanied by the presence of greater numbers of $CD8^+$ T cells in the systemic circulation, suggesting that $CD8^+$ T cells are activated by endogenous stimuli localized in the adipose tissue. Supporting this notion is our finding that obese adipose tissue induces $CD8^+$ T cell proliferation. The findings that incubation with $CD8^+$ T cells plus lean adipose tissue induced macrophage differentiation, although neither $CD8^+$ T cells nor lean adipose tissue did so alone, suggest that $CD8^+$ T cells and adipose tissue interact with each other to activate a local inflammatory cascade. In addition, the results of coculture experiments showing the interactions among $CD8^+$ T cells, macrophages and adipose tissue, as well as the results of our CD8 depletion experiments, which showed that $CD8^+$ T cells are essential for both the initiation and maintenance of adipose inflammation, strongly suggest that there is a relay involving both $CD8^+$ T cells and macrophages in obese adipose tissue that propagates local adipose inflammation.

In contrast to the increased infiltration of $CD8^+$ T cells, numbers of $CD4^+$ T cells and regulatory T cells were low at later time points (**Fig. 1**), which would also be expected to contribute to local inflammation within adipose tissue. For instance, subsets of $CD4^+$ T cells are known to secrete cytokines that can inhibit macrophage recruitment, including IL-4 and IL-10 (ref. 19), whereas regulatory T cells control adaptive immune responses by suppressing T cells, NK cells, NKT cells, B cells and dendritic cells[20]. In addition, regulatory T cells have also been shown to inhibit proinflammatory activation of monocytes[21] and to inhibit macrophage infiltration and renal injury in a model of chronic kidney disease[22]. It is therefore tempting to speculate that reducing the numbers of $CD4^+$ and regulatory T cells augments the inflammatory response during the late phase of adipose tissue obesity.

Taken together, our results support the idea that obese adipose tissue activates $CD8^+$ T cells, which, in turn, initiate and propagate inflammatory cascades, including the recruitment of monocytes and macrophages into obese adipose tissues and their subsequent differentiation and activation there. Thus, it seems that $CD8^+$ T cells have a primary role in obese adipose tissue inflammation, though future studies are needed to address which environmental cues within obese adipose tissue initiate $CD8^+$ cell infiltration. Even so, these results further support the idea that adipose inflammation has a major impact on systemic metabolism.

METHODS

Methods and any associated references are available in the online version of the paper at http://www.nature.com/naturemedicine/.

Note: Supplementary information is available on the Nature Medicine website.

ACKNOWLEDGMENTS

We gratefully acknowledge A. Matsuoka, X. Yingda, E. Magoshi, M. Hayashi, K. Wakabayashi, M. Tajima and Y. Yamazaki for excellent technical assistance. This study was supported by Research Fellowships from the Japan Society for the Promotion of Science for Young Scientists (S.N.), Grants-in-Aid for Scientific Research (I.M., R.N.) and grants for Translational Systems Biology and Medicine Initiative (R.N., T.K.) and Global Centers of Excellence program (R.N., T.K.) from the Ministry of Education, Culture, Sports, Science and Technology of Japan and a research grant from the National Institute of Biomedical Innovation (R.N.).

AUTHOR CONTRIBUTIONS

S.N. and M.N. performed *in vivo* and *in vitro* assays and analyzed all of the end points. K.H., K.U. and K.Y. performed human subject assays. S.N., I.M., K.E., H.Y., M. Otsu, M. Ohsugi, S.S., T.K. and R.N. supervised entire studies. S.N. and I.M. wrote the manuscript.

Published online at http://www.nature.com/naturemedicine/.
Reprints and permissions information is available online at http://npg.nature.com/reprintsandpermissions/.

1. Hotamisligil, G.S. Inflammation and metabolic disorders. *Nature* **444**, 860–867 (2006).
2. Weisberg, S.P. *et al.* Obesity is associated with macrophage accumulation in adipose tissue. *J. Clin. Invest.* **112**, 1796–1808 (2003).
3. Nishimura, S. *et al. In vivo* imaging in mice reveals local cell dynamics and inflammation in obese adipose tissue. *J. Clin. Invest.* **118**, 710–721 (2008).
4. Xu, H. *et al.* Chronic inflammation in fat plays a crucial role in the development of obesity-related insulin resistance. *J. Clin. Invest.* **112**, 1821–1830 (2003).
5. Savage, D.B., Petersen, K.F. & Shulman, G.I. Disordered lipid metabolism and the pathogenesis of insulin resistance. *Physiol. Rev.* **87**, 507–520 (2007).
6. Guilherme, A., Virbasius, J.V., Puri, V. & Czech, M.P. Adipocyte dysfunctions linking obesity to insulin resistance and type 2 diabetes. *Nat. Rev. Mol. Cell Biol.* **9**, 367–377 (2008).
7. Shoelson, S.E., Lee, J. & Goldfine, A.B. Inflammation and insulin resistance. *J. Clin. Invest.* **116**, 1793–1801 (2006).
8. Suganami, T., Nishida, J. & Ogawa, Y. A paracrine loop between adipocytes and macrophages aggravates inflammatory changes: role of free fatty acids and tumor necrosis factor alpha. *Arterioscler. Thromb. Vasc. Biol.* **25**, 2062–2068 (2005).

9. Wu, H. *et al.* T-cell accumulation and regulated on activation, normal T cell expressed and secreted upregulation in adipose tissue in obesity. *Circulation* **115**, 1029–1038 (2007).
10. Rausch, M.E., Weisberg, S., Vardhana, P. & Tortoriello, D.V. Obesity in C57BL/6J mice is characterized by adipose tissue hypoxia and cytotoxic T-cell infiltration. *Int. J. Obes. (Lond.)* **32**, 451–463 (2008).
11. Monney, L. *et al.* T_H1-specific cell surface protein Tim-3 regulates macrophage activation and severity of an autoimmune disease. *Nature* **415**, 536–541 (2002).
12. Brake, D.K., Smith, E.O., Mersmann, H., Smith, C.W. & Robker, R.L. ICAM-1 expression in adipose tissue: effects of diet-induced obesity in mice. *Am. J. Physiol. Cell Physiol.* **291**, C1232–C1239 (2006).
13. Traktuev, D.O. *et al.* A population of multipotent CD34-positive adipose stromal cells share pericyte and mesenchymal surface markers, reside in a periendothelial location and stabilize endothelial networks. *Circ. Res.* **102**, 77–85 (2008).
14. Nishimura, S. *et al.* Adipogenesis in obesity requires close interplay between differentiating adipocytes, stromal cells and blood vessels. *Diabetes* **56**, 1517–1526 (2007).
15. Cinti, S. *et al.* Adipocyte death defines macrophage localization and function in adipose tissue of obese mice and humans. *J. Lipid Res.* **46**, 2347–2355 (2005).
16. Sallusto, F., Lenig, D., Forster, R., Lipp, M. & Lanzavecchia, A. Two subsets of memory T lymphocytes with distinct homing potentials and effector functions. *Nature* **401**, 708–712 (1999).
17. Lumeng, C.N., Bodzin, J.L. & Saltiel, A.R. Obesity induces a phenotypic switch in adipose tissue macrophage polarization. *J. Clin. Invest.* **117**, 175–184 (2007).
18. Kintscher, U. *et al.* T-lymphocyte infiltration in visceral adipose tissue: a primary event in adipose tissue inflammation and the development of obesity-mediated insulin resistance. *Arterioscler. Thromb. Vasc. Biol.* **28**, 1304–1310 (2008).
19. Miller, R., Wen, X., Dunford, B., Wang, X. & Suzuki, Y. Cytokine production of $CD8^+$ immune T cells but not of $CD4^+$ T cells from *Toxoplasma gondii*-infected mice is polarized to a type 1 response following stimulation with tachyzoite-infected macrophages. *J. Interferon Cytokine Res.* **26**, 787–792 (2006).
20. Sakaguchi, S. *et al.* $Foxp3^+$ $CD25^+$ $CD4^+$ natural regulatory T cells in dominant self-tolerance and autoimmune disease. *Immunol. Rev.* **212**, 8–27 (2006).
21. Taams, L.S. *et al.* Modulation of monocyte/macrophage function by human $CD4^+CD25^+$ regulatory T cells. *Hum. Immunol.* **66**, 222–230 (2005).
22. Mahajan, D. *et al.* $CD4^+CD25^+$ regulatory T cells protect against injury in an innate murine model of chronic kidney disease. *J. Am. Soc. Nephrol.* **17**, 2731–2741 (2006).

ONLINE METHODS

Mice. We obtained Male C57BL/6J, *ob/ob* and *Cd8a*-deficient mice from Charles River Japan or Jackson Laboratories. All mice were housed under a 12-h light-dark cycle and allowed free access to food. To examine the time-course of changes in stromal vascular cell populations in adipose tissue under conditions of diet-induced obesity, we divided C57BL/6 mice into two groups and fed either a standard chow diet (6% fat, Oriental Yeast Company) or a high-fat diet (D12492, 60 Kcal% fat, Research Diets) from the age of 4 weeks.

To examine the effects of CD8 depletion on the initiation and development of adipose inflammation, we started antibody administration before the establishment of DIO. We fed male C57BL/6 mice a high-fat diet for 8 weeks, beginning when they were 4-weeks-old, and we intraperitoneally administered either CD8-specific antibody (3 μg per g body weight, 1 mg ml^{-1} solution, Biolegend) or control rat IgG (Sigma, 1 mg ml^{-1} PBS solution) weekly over the same period. We examined the mice at 12 weeks old (**Fig. 2** and **Supplementary Fig. 7**). We validated depletion of $CD8^+$ T cells by antibody as shown in **Supplementary Figure 11.**

To assess the effects of CD8 depletion on preestablished adipose inflammation in DIO mice, we fed C57BL/6 mice a high-fat diet, beginning when they were 9-weeks-old. Ten weeks later, we randomly assigned the 19-week-old obese mice to two groups and we intraperitoneally administered either CD8-specific antibody (120 μg per mouse) or control IgG three times per week for 2 weeks (total of six administrations). Age-matched lean C57BL/6 mice fed a normal chow diet served as controls. At 21 weeks, we performed oral glucose and insulin tolerance tests and then killed the mice for analysis of their adipose tissue (**Fig. 3** and **Supplementary Fig. 9**).

To assess the effects of CD8-deficient and adoptive transfer of $CD8^+$ T cells on adipose inflammation, we fed *CD8a*$^{-/-}$ mice either normal chow or a high-fat diet for 8 weeks, beginning when they were 6-weeks-old. We intravenously administered either 5×10^6 splenic $CD8^+$ T cells or control PBS weekly over the same period. We examined the *CD8a*$^{-/-}$ mice at 14-weeks-old. We prepared $CD8^+$ splenic T cells from 7-week-old C57BL/6 mice (**Fig. 4** and **Supplementary Fig. 10**). All experiments were approved by the Institutional Committee for Animal Research of The University of Tokyo and strictly adhered to the guidelines for animal experiments of The University of Tokyo.

Isolation of the stromal vascular fraction and flow cytometry. We isolated stromal vascular cells using previously described methods with some modifications. We killed the mice after general anesthesia after systemic heparinization. We removed the epididymal and subcutaneous adipose tissues and then minced it into small pieces (~2 mm). We vigorously agitated the pieces in PBS supplemented with 1 μg ml^{-1} heparin for 30 s to remove any circulating blood cells and then centrifuged the suspension at 1,000*g* for 8 min. We collected floating pieces of adipose tissue and incubated them for 20 min in collagenase solution (2 mg ml^{-1} of collagenase type 2 (Worthington) in Tyrode buffer (containing 137 mM NaCl, 5.4 mM KCl, 1.8 mM $CaCl_2$, 0.5 mM $MgCl_2$, 0.33 mM NaH_2PO_4, 5 mM HEPES and 5 mM glucose)) with gentle stirring. We then centrifuged the digested tissue again at 1,000*g* for 8 min. We resuspended the resultant pellet containing the stromal vascular fraction into PBS and filtered it through a 70-μm mesh. We washed the cells twice with PBS, incubated for 10 min in erythrocyte-lysing buffer (Becton Dickinson) as previously described[3], and we finally resuspended them in PBS supplemented with 3% FBS. We incubated these isolated cells with either labeled monoclonal antibody or isotype control antibody (eBioscience and BD Pharmingen) and analyzed by flow cytometry with a Vantage flow cytometer (Becton Dickinson) and FlowJo (Tree Star, Inc.) software. We used propidium iodide (Invitrogen) to exclude dead cells. We validated flow cytometric identification of M1 ($F4/80^+CD11c^+$) and M2 ($F4/80^+CD11c^-$) macrophages with CD11c markers as described in the **Supplementary Methods** and **Supplementary Figure 12.**

Immunohistochemistry. We stained and visualized whole-mount adipose tissue as previously described[14].

CFSE proliferation assay of $CD8^+$ T cells. We isolated splenic $CD8^+$ T cells from 7-week-old C57BL/6 mice and incubated the isolated $CD3^+$ $CD8^+$ cells with 5 μM CFSE (CellTrace CFSE Cell Proliferation Kit, Invitrogen). After staining, we incubated 2×10^5 cells in DMEM supplemented with 3% FBS for 2 d, with or without 20 mg of minced epididymal white adipose tissue prepared from either 20-week-old lean mice fed a normal chow diet or DIO mice fed a high-fat diet for 16 weeks. We harvested the $CD8^+$ cells and then analyzed them by flow cytometry to examine the proliferation status.

Differentiation of peripheral blood monocytes into macrophages. We isolated peripheral blood monocytes ($CD11b^{high}Gr\text{-}1^-$) from lean 7-week-old C57BL/6 mice. In the lower wells of a 24-well Multiwell Boyden chamber (Becton Dickinson), we cultured 5×10^4 monocytes per well in DMEM supplemented with 3% FBS, with or without 10 mg of minced epididymal adipose tissue prepared from 7-week-old lean mice in the upper wells. Also in the upper wells, we cultured 5×10^4 $CD3^+CD8^+CD4^-$ T cells, which we isolated from epididymal adipose tissues of 20-week-old lean or DIO mice. We incubated the cells for 7 d, after which the cells in the upper wells were collected, stained for CD11b, F4/80 and CD68, and assayed by flow cytometry for the differentiated macrophage fractions ($CD11b^+F4/80^+CD68^+$).

Migration of RAW264.7 and peritoneal macrophages. We isolated $CD8^+$ T cells from blood collected from C57BL/B6J mice after cardiac puncture. We isolated and cultured $CD3^+CD8^+$ cells were in DMEM supplemented with 3% FBS. To activate $CD8^+$ T cells, we cultured the cells with recombinant IL-2 (20 U ml^{-1}; Sigma), Dynabeads CD3/CD28 T Cell Expander (a bead-to-cell ratio of 1:1) and 2-mercaptoethanol (50 μM). After 120 h of culture, we aspirated the culture medium and performed migration assay using Boyden chambers with 8-μm pore inserts (Becton Dickinson). We cultured RAW264.7 and peritoneal macrophages in the upper wells, and we added the conditioned medium to the lower wells. We used fresh DMEM supplemented with 5% FBS as a control. To inhibit MCP-1 activity, we added a neutralizing antibody (5 μg ml^{-1} antibody to MCP-1, clone 2H5, Biolegend) to the conditioned medium.

TNF-α production in macrophages cocultured with $CD8^+$ cells. We isolated $F4/80^+$ $CD11b^+$ macrophages from epididymal adipose tissue from lean 7-week-old C57Bl/B6J mice, and we isolated $CD3^+CD8^+CD4^-$ T cells from epididymal adipose tissue from 20-week-old lean or DIO mice. We then added the adipose macrophages to the upper wells of a Multiwell Boyden chamber (Becton Dickinson) (5×10^4 cells per well), and we added the same number of $CD8^+$ T cells to the lower wells, after which we cultured the cells in DMEM supplemented with 3% FBS for 7 d. We assessed intracellular production of TNF-α by flow cytometry using an intracellular cytokine production detection kit (Cytofix/Cytoperm Fixation/Permeabilization Solution Kit, BD Pharmingen).

Human subjects. We acquired subcutaneous adipose tissue from healthy female donors undergoing liposuction of the abdomen or thighs (after obtaining their consent). We examined expression of *CD8a* in the tissue. We processed samples comprised of 1 g of each specimen by digestion with collagenase and then centrifuged to isolate the stromal vascular fractions. We purified total RNA using Trizol (Invitrogen) and determined relative mRNA levels using real-time PCR. This study was approved by the Ethics Committee of The University of Tokyo Hospital.

Statistical analyses. We expressed the results as means ± s.e.m. We determined the statistical significance of differences between two groups using Student's *t* tests, and we evaluated differences among three groups by analysis of variance followed by *post-hoc* Bonferroni tests. Values of $P < 0.05$ were considered significant.

Reconsideration of Insulin Signals Induced by Improved Laboratory Animal Diets, Japanese and American Diets, in IRS-2 Deficient Mice

Authors

H. Hashimoto[1], T. Arai[2], A. Mori[2], K. Kawai[1], K. Hikishima[1, 5], Y. Ohnishi[1], T. Eto[1], M. Ito[1], K. Hioki[1], R. Suzuki[3], M. Ohsugi[3], M. Saito[1], Y. Ueyama[4], H. Okano[5], T. Yamauchi[3], N. Kubota[3], K. Ueki[3], K. Tobe[3], N. Tamaoki[1], T. Kadowaki[3], K. Kosaka[1, 3]

Affiliations

Affiliation addresses are listed at the end of the article

Key words
- adipocytokines
- obesity
- fatty acid synthesis
- metabolic features
- diabetes
- autoimmunity

Abstract

Current Japanese and American diets and Japanese diet immediately after the War were converted to laboratory animal diets. As a result, current laboratory animal diet (CA-1, CLEA) unexpectedly resembled the diet of Japanese after the War. This is considered to result in an under-evaluation of diabetes research using laboratory animals at present. Therefore, changes in insulin signals caused by current Japanese and American diets were examined using *IRS-2* deficient mice (*Irs2*$^{-/-}$ mice) and mechanisms of aggravation of type 2 diabetes due to modern diets were examined.

Irs2$^{-/-}$ mice at 6 weeks of age were divided into three groups: Japanese diet (Jd) group, American diet (Ad) group and CA-1 diet [regular diet (Rd)] group. Each diet was given to the dams from 7 days before delivery. When the *Irs2*$^{-/-}$ mice reached 6 weeks of age, the glucose tolerance test (GTT), insulin tolerance test (ITT) and organ sampling were performed. The sampled organs and white adipose tissue were used for analysis of RNA, enzyme activity and tissues. In GTT and ITT, the Ad group showed worse glucose tolerance and insulin resistance than the Rd group. Impaired glucose tolerance of the Jd group was the same as that of the Rd group, but insulin resistance was worse than in the Rd group. These results were caused an increase in fat accumulation and adipocytes in the peritoneal cavity by lipogenic enzyme activity in the liver and muscle, and the increase in TNFα of hypertrophic adipocyte origin further aggravated insulin resistance and the increase in resistin also aggravated the impaired glucose tolerance, leading to aggravation of type 2 diabetes. The Japanese and American diets given to the *Irs2*$^{-/-}$ mice, which we developed, showed abnormal findings in some *Irs2*$^{-/-}$ mice but inhibited excessive reactions of insulin signals as diets used in ordinary nutritional management.

received 09.02.2009
first decision 18.05.2009
accepted 27.05.2009

Bibliography
DOI 10.1055/s-0029-1225352
Published online: 2009
Exp Clin Endocrinol Diabetes

ISSN 0947-7349

Correspondence
H. Hashimoto
Department of Laboratory Animal Research
Central Institute for Experimental Animals
Tel.: +044/754/44 85
Fax: +044/751/88 10
hashimot@ciea.or.jp

Introduction

Type 2 diabetes mellitus appears to be increasing mainly in the United States, Africa and Asia. In 2000 there were one hundred and fifty million Type 2 diabetic patients, but they are predicted to increase substantially to two hundred and twenty million world-wide in 2010 [37]. Since World War II (WWII), type 2 diabetic patients have increased markedly with dramatic changes of lifestyle in Japan. Typical changes of the lifestyle include the increases in high fat diets, sedentary habits and driving. Especially, the level of fat in modern Japanese diets increased from 20.0 g/day in 1953 to 59.9 g/day in 1995 according to the nation-wide nutrition monitoring survey in Japan. In addition, the Japanese population is predisposed to develop type 2 diabetes due to insufficient insulin secretion in spite of no predisposition to obesity.

Human type 2 DM is characterized by peripheral insulin resistance and defective insulin secretion [11, 12]. It is known that type 2 DM is associated with disorders of insulin receptor substrates (IRS), which mediate pleiotropic signals initiated by receptors for insulin and adipokines [7, 13, 24, 26, 27] secreted from adipocytes. In IRS family [22, 31], *IRS-2* deficient (*Irs2*$^{-/-}$) mice develop diabetes presumably due to inadequate β cell proliferation [14] and increased adiposity [32] combined with insulin resistance. In fact, insulin resistance in *Irs2*$^{-/-}$ mice is ameliorated, at least in part, by reducing the adiposity [28]. Therefore, we thought that *IRS-2* is the central signal in glucose homeostasis. Hashimoto et al. (2006) [5] backcrossed the *IRS-2* deficient mice

Table 1 Conversion from nutrition in human to nutrition contents for laboratory animals.

(a)

	Calorie	Modern American diet[1] Intake weight (kcal/day) 2409.1→462.9[4] Intake weight (g/day)	Modern American diet[1] Relative value (%) 118.7 kcal (%)	Modern Japanese diet[2] Intake weight (kcal/day) 1985.1→384.9 Intake weight (g/day)	Modern Japanese diet[2] Relative value (%) 98.7 kcal (%)	Japanese diet after WWII[3] Intake weight (kcal/day) 390.0 Intake weight (g/day)	Japanese diet after WWII[3] Relative value (%) 100.0 kcal (%)
	protein	94.9→18.2	15.8	81.5→15.8	16.4	69.0→13.0	13.3
	fat	92.7→17.8	34.6	59.9→11.6	27.2	20.0→3.8	8.7
	total weight	85.5→16.4	31.9	56.9→11.0	25.8	19.0→3.6	8.3
	SFA	31.3→6.0	11.7	16.0→3.1	7.2	4.3→0.8	1.9
fatty acid	MUFA	35.8→6.9	13.4	20.5→4.0	9.3	6.0→1.1	2.6
	PUFA	18.4→3.5	6.9	20.3→3.9	9.2	8.7→1.6	3.8
	moisture	298.8→57.4	49.6	280.0→54.3	56.4	403.0→76.0	77.9

(b)

	Modern American diet	Modern Japanese diet	Japanese diet after WWII	CA-1
moisture (%)	8.8	10.0	11.1	8.3
crude protein (%)	24.3	22.5	20.2	26.8
crude fat (%)	**15.5**	**10.1**	**3.9**	**5.0**
crude fiber (%)	5.4	5.2	5.2	3.4
crude ash (%)	6.4	6.1	6.2	7.6
NFE (%)	39.6	46.2	53.2	48.9
calorie (kcal/100 g)	395.1	365.0	328.9	347.4
fat energy (%)	35.4	24.8	10.7	–
CP energy (%)	24.6	24.6	24.5	–

[1] USDA data (1994–96)
[2] Nation wide nutrition monitoring survey in Japan (1995)
[3] Nation wide nutrition monitoring survey in Japan (1953)
[4] Conversion from human to mice
SFA: Saturated Fatty Acids
MUFA: Monounsaturated Fatty Acids
PUFA: Polyunsaturated Fatty Acids

(C57BL/6×CBA hybrid background) generated by Kubota et al. (2000) [14] with C57BL/6JJcl mice to establish an inbred line of *IRS-2* deficient mice (*Irs2*$^{-/-}$ mice). As a result, *IRS-2* deficient mice with C57BL/6JJcl genetic background at the age of 6 weeks showed profiles compatible with several features of the metabolic syndrome, including hyperglycemia, hyperinsulinemia, insulin resistance, hypertriglyceridemia, and high FFA when compared with *IRS-2* deficient mice with a C57BL/6×CBA hybrid background.

Diets with excessive fat as a load factor, for example more than 30%, have been fed to various models to show the relation of between type 2 diabetes mellitus and lipid metabolism in many experiments. However, most regular diets fed to type 2 diabetic model mice contain about 5% fat in usual breeding, although one of the factors increasing Japanese type 2 diabetes patients is high fat diets. Therefore, we converted the nutrient content of regular diet for laboratory animals to the human nutrient content on the basis of the nation-wide nutrition monitoring survey in Japan and the National Research Council in the United States. As a result, the nutrient content of CA-1 (CLEA, Tokyo, Japan) as a regular diet became similar to that of the Japanese diet after the WWII. Conversely, the results of converting the nutrient content of modern Japanese and American diets to laboratory animal diets indicated that the fat levels were two or three times higher than that of regular diet such as CA-1. These differences of fat levels suggest the possibility of underestimates of experimental results using various diabetic mice and overlooking of important signals when breeding with regular diets. Therefore, we produced laboratory animal diets that imitated modern Japanese and American diets, and investigated the effects on characteristics of plasma adipokines, metabolites and enzyme activities in *Irs2*$^{-/-}$ mice.

Material and Methods

Animals

IRS-2 deficient mice generated by Kubota et al. (2000) [14] were backcrossed with the original C57BL/6JJcl genetic background (*Irs2*$^{-/-}$ mice) for more than 10 generations. *Irs2*$^{-/-}$ mice were prepared by crossing with *Irs2*$^{-/-}$ mice, which were used for *in vitro* fertilization and embryo transfer. *Irs2*$^{-/-}$ mice were divided to 3 groups, a regular diet (regular diet (Rd) group), Japanese diet (Japanese diet (Jd) group), and American diet (American diet (Ad) group) at the age of 4 weeks. These diets were fed to *Irs2*$^{-/-}$ mice since the embryos were transferred to pseudo pregnant MCH (ICR) mice. *Irs2*$^{-/-}$ mice were housed in Pair Mex II (Osaka Micro system, Osaka, Japan) at the age of 4 weeks, and provided

with regular and Japanese, and American diets as well as tap water *ad libitum*. At the age of 5 weeks, intake rhythm of *Irs2*$^{-/-}$ mice was synchronized with two *Irs2*$^{-/-}$ mice near the average intake weight and pattern in each group. The animal room and specific pathogen-free conditions were the same as previous study [5]. This study was approved by the Animal Committee of the Central Institute for Experimental Animals (Permit No. 06023).

Design of modern Japanese and American diets

Calorie levels for laboratory animal diet (390 kcal/100 g, referenced to NRC, 1995) were based on human Japanese diet after WWII (**Table 1a**). Total calories in human Japanese diet after WWII were taken as a relative value of 100, multiplied by 390 kcal/100 g for both modern Japanese and American diets. Calorie levels in nutrient content of each diet were converted to weight (g)/100 g. As a result of these conversions, these diet contents presented two problems, 1) protein level (percentage of protein calories) was too low, and 2) total levels of protein, fat, and moisture were too high. We thought that these problems might induce inferior growth of infants. These problems were solved by decrease of moisture, increase of protein, and maintenance of fibrous and mineral contents in nutrient combinations. As a result, the practical combination rates of materials and nutrient content are shown in **Table 1b.** The differences between conversion values and practical combination rates of materials were calories and moisture to protect the growth of infants. The nutrient content of regular diet, CA-1, was similar to that of Japanese diet after WWII for laboratory animals. Therefore, we substituted the Japanese diet after WWII for CA-1 as the control in this study.

In vivo Glucose Homeostasis and Chemical analysis

At the age of 6 weeks, glucose tolerance test (GTT), insulin tolerance test (ITT), and harvests of blood, liver, femoral muscles (skeletal muscle), white adipose tissue (WAT), and pancreas for chemical analysis. These protocol and condition were the same as previous study [5].

Plasma glucose concentrations were assayed by the glucose oxidase method [8]. Plasma triglyceride, FFA, and total cholesterol levels were measured using commercially available kits (Wako Pure Chemical Industries, Tokyo, Japan). Plasma insulin was assayed using immunoreactions according to Arai et al. (1989) [1]. Plasma TNFα (eBioscience, California, USA), resistin (AdipoGen, Seoul, Korea), MCP-1 (Pierce Biotechnology, Inc., Rockford, Illinois, USA), and leptin (Ray Biotech, Inc., Norcross, Gergia, USA) were assayed by commercially available ELISA kits.

Isolation of cytosol fractions from the excised tissues [33], and activity assays of hexokinase [34], glucokinase [34], pyruvate kinase [6], aspartate aminotransferase [18], ATP citrate lyase [30], fatty acid synthase [4], and malic enzyme [16] were performed as reported previously.

RNA preparation and Quantitative Real-Time PCR

Total RNA was extracted from liver, skeletal muscle, WAT, and pancreas of *Irs2*$^{-/-}$ mice using TRizol reagent (Invitrogen) following the manufacturer is instructions. RNA (Liver: 500 ng, others: 50–100 ng) was then reverse-transcribed to cDNA using Super Script III RNaseH$^-$ reverse transcriptase (Invtrogen). Real-Time quantitative PCR were carried out with the SYBR Premix Ex Taq™ (TaKaRa) and specific primers for SREBP-1c (Forward: 5′ GGTGTATTTGCTGGCTTGGT 3′ and Reverse: 5′ ACTAATGGGCCCTGATCCTT 3′), PPAR γ 2(Forward: 5′ GGTGAAACTCTGGGAGATTC 3′ and Reverse: 5′ TAATAAGGTGGAGATGCAGG 3′), GLUT2 (Forward: 5′ GGCTAATTTCAGGACTGGTT 3′ and Reverse: 5′ TTTCTTTGCCCTGACTTCCT 3′), GLUT4 (Forward: 5′ TCATTCTTGGACGGT TCCTC 3′ and Reverse: 5′ AGAATCAGCTGCAGGAGAGC 3′) and β actin (Forward: 5′ ACGGGCATTGTGATGGACTC 3′ and Reverse: 5′ GTGGTGGTGAAGCTGTAGCC 3′) according to the manufacturer's instructions. The PCR reactions and detection were performed on a ABI PRISM 7700 using β actin as internal control for normalization purposes.

In addition, reverse transcription (RT)-PCR also was performed to confirm the results of quantitative Real-Time PCR visually followed to PCR conditions according to the manufacturer's instructions. PCR amplification was carried out for 25–35 cycles, consisting of 95 for 30 s, 63.4 °C(SREBP-1c), 59.1 °C(PPARγ2), 64.0 °C(GLUT2), 65.0 °C(GLUT4), or 68.0 °C(ßactin) for 30–40 s, and 72 °C for 5 min in 20 µl of reaction mixture containing 1.5 mM Mg^{2+} and Ex-Tac (TaKaRa, Kyoto).

Histological analysis of liver, WAT, and pancreatic β cells

The liver and WAT were fixed in 10% buffered formalin and embedded in paraffin. Sections of islets were stained with hematoxylin and eosin. Immunohistochemistry of pancreatic β cells was made according to Arai et al. (2008) [2].

Magnetic Resonance Imaging (MRI)

Mice were scanned using 7T Bruker MRI under isoflurane anesthesia. Whole-body was imaged for each mouse in accordance with a fat MRI protocol. Parameters for short T_1-weighted spin-echo pulse sequence were: repetition time = 310 ms, echo time = 14.7 ms, slice thickness = 1.2 mm, field-of-view = 2.6 × 2.6 $(cm)^2$, matrix size = 192 × 192, average = 6. A fat image region was evaluated with visual inspection.

Results

Body Weights

Body weights of Rd, Jd and Ad group at 6 wk of age were 20.8 ± 0.4 g (Mean ± SEM), 22.7 ± 0.5 g and 22.9 ± 0.5 g each. Japanese and American diet increased the body weights of *Irs2*$^{-/-}$ mice when compared with regular diet ($p < 0.05$–0.01).

Glucose tolerance test

Fig. 1a shows the results of GTT in *Irs2*$^{-/-}$ mice fed modern Japanese and American diets for laboratory animals. Blood glucose concentrations before and after glucose loading differed significantly ($p < 0.05$) between the Rd group and Ad group, although not between the Rd group and Jd group. Thereafter, the Ad group continued to maintain severly impaired glucose tolerance ($p < 0.05$).

Insulin tolerance test

Fig. 1b shows the results of ITT of *Irs2*$^{-/-}$ mice fed modern Japanese and American diets for laboratory animals. Blood glucose concentrations before insulin injection were already significantly higher in the Jd group and Ad group than in the Rd group ($p < 0.05$). The glucose concentration-lowering effect of insulin was significantly impaired in the Jd group and Ad group compared with the Rd group ($p < 0.05$–0.01), suggesting that the Jd group and Ad group show deterioration of insulin resistance.

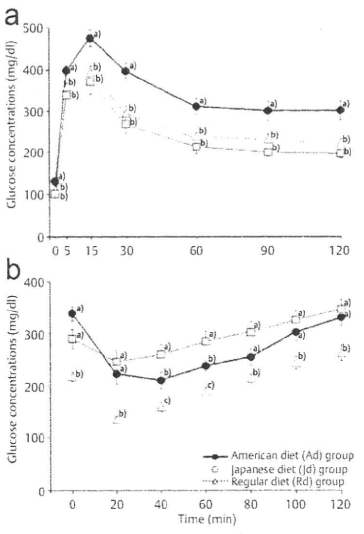

Fig. 1 Effects of modern Japanese and American diets on impaired glucose tolerance and insulin resistance in *Irs2*$^{-/-}$ mice. (**a**) Glucose tolerance test, (**b**) Insulin tolerance test Less than $p<0.05$: a) vs. b), b) vs. c), a) vs. c); ANOVA and Tukey's test.

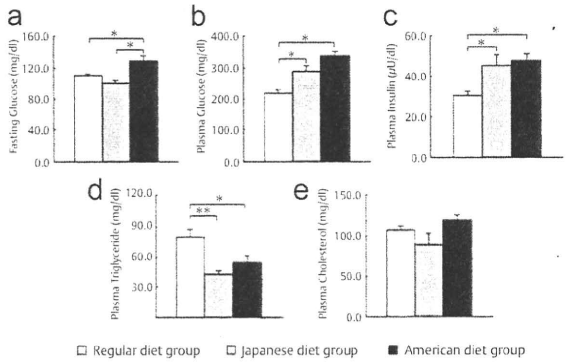

Fig. 2 Effects of modern Japanese and American diets on plasma metabolites in *Irs2*$^{-/-}$ mice. (**a**) Fasting glucose, (**b**) plasma glucose, (**c**) plasma insulin, (**d**) plasma triglyceride, and (**e**) plasma cholesterol. Data are presented as mean ± standard error. *: $p<0.05$, **: $p<0.01$ (ANOVA and Tukey's test).

Plasma metabolites

The Ad group showed increased plasma fasting glucose concentration (○ **Fig. 2a**) compared with other groups ($p<0.05$). However, plasma glucose (○ **Fig. 2b**) and insulin concentrations (○ **Fig. 2c**) in the Jd and Ad groups were increased when compared with the Rd group ($p<0.05$). Conversely, plasma triglyceride concentrations (○ **Fig. 2d**) in the Jd and Ad groups were decreased as compared with the Rd group ($p<0.05$). Plasma cholesterol concentration (○ **Fig. 2e**) was the same in the Jd and Ad groups.

Effects of Japanese and American diets on the liver

Expression of SREBP-1c mRNA (○ **Fig. 3a**) in the Ad group was increased compared with the Rd group ($p<0.05$). In addition, expressions of PPAR γ 2 mRNA (○ **Fig. 3b**) and GLUT2 mRNA (○ **Fig. 3c**) in the Ad group were higher than in other groups ($p<0.05$).

Cytosolic glucokinase (○ **Fig. 3d**), pyruvate kinase (○ **Fig. 3e**), and PEPCK activities (○ **Fig. 3f**) were not altered by the differences of diet. Cytosolic fatty acid synthase activities (○ **Fig. 3g**) of the Jd and Ad groups were decreased compared with the Rd group ($p<0.05$). However, ACL activities (○ **Fig. 3h**) of the Ad group increased compared with other groups ($p<0.05$). In addition, malic enzyme (○ **Fig. 3i**) of both the Jd and Ad groups also increased when compared with the Rd group ($p<0.05$). Cytosolic aspartate aminotransferase activities (○ **Fig. 3j**) of the Ad group increased ($p<0.05$), in spite of hepacytes of the Ad group at 6 wk did not differ from the Rd group by histopathologic examination (○ **Fig. 3k**).

Effects of Japanese and American diets on skeletal muscle

Expressions of GLUT4 mRNA (○ **Fig. 4a**) in the Jd and Ad groups were lower than that in the Rd group ($p<0.01$).

Cytosolic hexokinase (○ **Fig. 4b**), glucose-6-phosphate dehydrogenase (○ **Fig. 4b**), ATP citrate lyase (○ **Fig. 4e**) and malic enzyme (○ **Fig. 4f**) were not altered by differences in diet. Cytosolic fatty acid synthase (○ **Fig. 4c**) of the Jd group showed higher activity than in the Rd group ($p<0.05$).

Effects of Japanese and American diets on WAT

Expression of GLUT4 mRNA (○ **Fig. 5a**) was not changed in each group. Expression of PPAR γ 2 mRNA (○ **Fig. 5b**) in the Jd and Ad groups was higher than that in the Rd group ($p<0.05$–0.01).

Both the Jd and Ad groups showed increased plasma TNFα concentrations (○ **Fig. 5c**) compared with the Rd group ($p<0.05$). In addition, the Ad group showed increased plasma resistin concentrations (○ **Fig. 5d**) compared with other groups ($p<0.05$). However, plasma MCP-1 concentrations (○ **Fig. 5e**) were not altered. On the other hand, both Jd and Ad groups showed decreased plasma adiponectin concentrations (○ **Fig. 5f**) compared with the Rd group ($p<0.05$). The Ad group showed increased plasma leptin concentrations (○ **Fig. 5g**) compared with the Rd group ($p<0.05$). Both the Jd and Ad groups showed decreased plasma FFA concentrations (○ **Fig. 5h**) compared with the Rd group ($p<0.05$–0.01).

MRI showed the effects of Japanese and American diets on intraperitoneal WAT in *Irs2*$^{-/-}$ mice (○ **Fig. 6a, b**). Peritoneal WAT was accumulated in mice on Japanese and American diets. WAT around the kidney and testes in the Jd and Ad groups increased in proportion to fat contents of diets when compared with the Rd group. In addition, the Jd and Ad groups were corpulent when compared with the Rd group (○ **Fig. 6c**).

Effects of Japanese and American diets on the pancreas

Expression of GLUT2 mRNA (○ **Fig. 7a**) in the Ad group was the lowest among all groups ($p<0.05$). The Jd and Ad groups showed hyperinsulinemia when compared with the Rd group ($p<0.05$). The rates of increases of insulin concentration in each group after glucose load were the same, but insulin in the Am group at 30 min after glucose load was maintained of higher concentrations than that in other groups ($p<0.05$) (○ **Fig. 7b**). On histopathologic examination of Langerhans' islands, insulin secretion was observed in all three groups (○ **Fig. 7c**).

Discussion

Takahashi et al. (1999) reported that fat content in diets causing impaired glucose tolerance in C57BL/6J mice was a calorie ratio exceeding 40% [29]. Thereafter, high fat diets inducing diabetes in mouse strains have fat contents usually exceeding 40% and as